

Finding order in complexity: A study of the fluid dynamics in a three-dimensional branching network

Abhijit Guha, Kaustav Pradhan, and Prodosh Kumar Halder

Citation: *Phys. Fluids* **28**, 123602 (2016); doi: 10.1063/1.4971315

View online: <http://dx.doi.org/10.1063/1.4971315>

View Table of Contents: <http://aip.scitation.org/toc/phf/28/12>

Published by the [American Institute of Physics](#)

Articles you may be interested in

[Aerodynamics of two-dimensional flapping wings in tandem configuration](#)

Phys. Fluids **28**, 121901 (2016); 10.1063/1.4971859

[The minimal flow unit in complex turbulent flows](#)

Phys. Fluids **28**, 125102 (2016); 10.1063/1.4968827

[A statistical model to predict streamwise turbulent dispersion from the wall at small times](#)

Phys. Fluids **28**, 125103 (2016); 10.1063/1.4968182

[Numerical simulations of the breakup of emulsion droplets inside a spraying nozzle](#)

Phys. Fluids **28**, 123103 (2016); 10.1063/1.4972097

Finding order in complexity: A study of the fluid dynamics in a three-dimensional branching network

Abhijit Guha,^{a)} Kaustav Pradhan, and Prodosh Kumar Halder

*Mechanical Engineering Department, Indian Institute of Technology Kharagpur,
Kharagpur 721302, India*

(Received 25 June 2016; accepted 17 November 2016; published online 20 December 2016)

The complex fluid dynamics associated with the flow in three-dimensional dichotomously branching networks is investigated. The flow physics described here is generic, though the particular flow geometry employed represents a model human bronchial tree. Up to six generations of branches (involving 63 straight portions and 31 bifurcation modules) are computed in one go; such computational challenges are rarely taken in the literature. In the present study, two branching configurations are considered side by side: the most widely studied in-plane configuration in which the centrelines of all generations lie on the same plane, and the 90° out-of-plane configuration in which the centreline of each generation is rotated with respect to its grandmother generation following a systematic methodology to form a space-filling three-dimensional structure. The paper develops a physical understanding of the fluid dynamics of branching networks and its dependence on the configuration (in-plane versus out-of-plane) and the extent (four, five, or six generations) of the network under consideration. The study of co-planar vis-à-vis non-planar configurations establishes a quantitative evaluation of the dependence of the fluid dynamics on the three-dimensional arrangement of the same individual branches. It is shown that apparent symmetry in the geometry of any two branches does not automatically imply symmetry in the flow field in those two branches. With the help of velocity contours, pressure contours, and distribution of mass flow in each branch, a qualitative and quantitative study is performed on the nature and evolution of flow asymmetry. The computations show that the degree of mass-flow asymmetry is smaller for the out-of-plane configuration (which is a more realistic model of a human bronchial tree) as compared to that for the in-plane configuration. The mass-flow asymmetry grows in each successive generation (starting from generation G2 for in-plane and G3 for out-of-plane configurations). In addition to mass-flow distribution, other types of asymmetries in the flow field are also analysed. It is established that, in spite of the complexity of the flow solutions, there also exists a systematic order such that it is possible to ascertain the flow field in all branches of a particular generation by determining the flow field in some systematically selected branches of that generation, indicating a possible route to the saving of computational resource and time. *Published by AIP Publishing.* [<http://dx.doi.org/10.1063/1.4971315>]

I. INTRODUCTION

The main objective of this paper is to study and understand the physics of fluid flow through complex three-dimensional internal passages formed by a dichotomously branching network. Such a network is found in several biological systems, the human bronchial tree being an important example. Such a network may also be relevant for future engineered small-scale or micro systems based on fractal or other geometrical algorithms. (Ref. 1 discusses an example of a novel heat

^{a)} Author to whom correspondence should be addressed. Electronic mail: a.guha@mech.iitkgp.ernet.in

exchanger for a hypersonic engine, its bio-inspired design being based on the fish-gill morphology.) This paper adopts the human bronchial tree for specifying the geometry and dimensions of the computational passages in which the fluid dynamics is studied. Now, the geometry of the bronchial tree may either be constructed by various models or by taking morphological data directly from CT-scan images of individuals; both types of research are discussed below. The limited number of works involving CT-scan data obviously reports more realistic results, but applies to specific individuals and does not contain any detailed fluid dynamic interpretation. The majority of the published studies use generalized geometric models, which is also the line taken here. The number of branches in a dichotomous network increases rapidly according to the formula $2^n - 1$, where n is the number of generation considered. The computations given in most of the references are restricted to three or four generations. In the present work, up to six generations of branches are computed in one go (involving 63 branches with many complex three-dimensional bifurcation units connecting the cylindrical portions); such computational challenges are rarely taken in the literature, particularly while analyzing the fluid dynamics in such fine details. The focus of the present study is therefore kept on the inspiratory flow; inclusion of the detailed fluid dynamics of expiratory or time-varying flow in a single paper would make it impractically long.

The inspiration for the study of fluid flow in the human bronchial tree originates from the fact that the fluid flow by itself is responsible for the gaseous exchange processes as well as it, in turn, determines the transport of inhaled particles and their deposition at various locations. The particles (which may contain pathogens) may be inhaled unintentionally as being part of the inhaled air or deliberately for the treatment of diseases (e.g., asthma). The knowledge of particle transport and deposition in the bronchial tree is therefore important for understanding (and perhaps controlling) the causation of certain diseases and for targeted drug delivery. Guha² formulated a unified theory for the deposition of particles, which applies to various flow regimes and particle sizes (from the nanometer to millimeter), and reproduces the experimental results closely. A lucid but comprehensive description of the flow of fluid and particles in the human bronchial tree is given by Guha.³

A number of models have been proposed for the human bronchial tree.⁴⁻⁶ The Weibel model⁴ is the simplest and the most explored of all. According to Weibel,⁴ the bronchial tree (originating from the trachea and ending in the alveolar sacs) comprises 23 generations of dichotomously branching airways (that amounts to $2^{23} - 1$ branches). A single computation covering the entire bronchial tree is computationally resource intensive. Many previous works have therefore simulated only part of the bronchial tree without a comprehensive evaluation of such segmentation on the overall accuracy of the results.⁷⁻⁹ Nowak *et al.*,⁷ used a 3.5 generation sub-unit model to study the fluid dynamics in up to 23 generations of a symmetric model. Kleinstreuer and Zhang⁸ used adjustable triple bifurcation units (TBUs) to represent the particle deposition in a 16-generation model of the tracheobronchial tree. Walters and Luke⁹ developed a flow path ensemble method using stochastic coupling approach to determine the flow features in generations 4-12 of Weibel's model.

Several other studies have also been carried out that consider the fluid flow in symmetric branching networks. Zhao and Lieber^{10,11} performed comprehensive experiments to study the velocity profiles obtained in a single bifurcation for both steady inspiratory and expiratory flows. Following this, Zhao *et al.*¹² gave numerical solutions to the problem of flow in a single symmetric bifurcation which matched well with their experimental results. Tadjfar and Smith¹³ performed direct numerical simulations (DNSs) and slender flow modelling on a single mother tube of circular cross section branching into two equal but diverging daughter tubes of semi-circular cross section. Kang *et al.*¹⁴ analysed the effect of geometric variations on the pressure loss across a single bifurcation. Comer *et al.*¹⁵ studied the air flow in symmetric branching networks comprising three generations. The influence of the inlet velocity profile on the flow characteristics in a three-generation network was studied by Zhang *et al.*¹⁶ Liu *et al.*¹⁷ investigated the pressure loss and asymmetric mass-flow distribution in a three-generation branching network. Zhang *et al.*¹⁸ considered the flow in symmetric triple bifurcations of the human bronchial tree. All these studies¹⁵⁻¹⁸ considered the intermediate branches of the bronchial tree. For example, the network considered by Liu *et al.*¹⁷ comprised generations G5-G7. While generation G5 consists of 32 branches in the bronchial tree, the geometry employed in Ref. 17 considers only one. It has been established here that even for

a symmetric bronchial tree network, the mass-flow distribution among the branches of a particular generation is non-uniform from the third generation onwards. Therefore, a study considering the intermediate segments of the bronchial tree (G5-G7) may not be able to capture the complete flow physics that would actually be found in a network containing all branches of the generations considered.

Studies of fluid flow and particle deposition in patient-specific CT-scanned respiratory airways have also been carried out by some researchers. Luo and Liu¹⁹ considered turbulent inspiratory flow characteristics in five generations of a CT-scanned human lung model. Pourmehran *et al.*²⁰ simulated air flow and magnetic particle deposition in the bronchial geometry obtained from the CT-scan images of a 48 year old healthy female. Banko *et al.*²¹ experimentally studied the steady inspiratory flow in an anatomically accurate model of the bronchial tree obtained from CT-scan images of a 47 year old healthy male. Since studies based on CT-scan data apply to specific individuals, most of the fluid dynamic studies use generalized geometric models. The present fluid dynamic study also uses one such generalized model of the bronchial network.

A model bronchial tree network is constructed by successively connecting cylindrical sections representing the bronchial airways of a particular generation with those of the next generation through transition zones which are referred to here as bifurcation modules. The model network adopted for the present study follows the symmetric dichotomous branching proposed by Weibel.⁴ A schematic diagram of a generic bifurcation module, in the context of the adjoining generations of cylindrical sections, is shown in Figure 1. The figure shows the qualitative constructional details of a bifurcation module, with the required variation of cross-sectional shape and area in the directions of the primary flows, such that a smooth transition is possible from the larger cylindrical cross section of the $n - 1$ generation to the smaller cylindrical cross section of the n -th generation. For dichotomous branching, a bifurcation module connects the end of a cylindrical section (representing the ‘mother’ branch for this module) to the beginning of two cylindrical sections (representing the ‘daughter’ branches). The cross-sectional shape of the bifurcation module is circular at the beginning at section 1-1' (so that it can seamlessly merge with the cylindrical section of the preceding generation). Then the shape changes in a complex fashion, documented at representative sections in Figure 1, finally being circular again at sections 5-5' and 6-6' in order to seamlessly merge with the two cylindrical sections of the next generation.

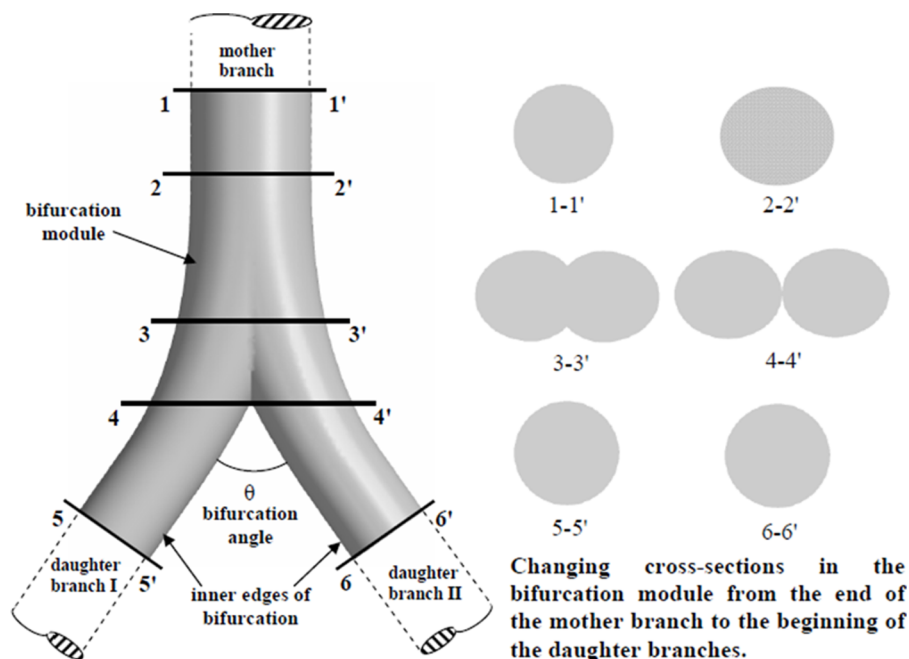


FIG. 1. Schematic details of a typical bifurcation module.

A particular generation in the bronchial tree network is referred to here by the symbol G_n , where the index n progressively takes the integer values 0, 1, 2, etc., the number 0 being assigned to the trachea which is the first branch of the network. Therefore, as an example, a four-generation network would consist of the generations G_0 , G_1 , G_2 and G_3 . The data given by Weibel⁴ for generations G_0 - G_5 are reproduced in Table I. However, Weibel did not specify the bifurcation angle between the two daughter branches emanating from the same mother branch. Based on an extensive review of other previous studies,^{10,11,17,22} the value of bifurcation angle is set at 70° for the illustrative computations reported in this study.

For the in-plane configuration of the bronchial tree network, the centrelines of all the bifurcation modules and the cylindrical sections of all generations lie on a single plane (which is denoted by the term “meridional plane” in this paper). It is to be realised that, in the in-plane configuration, although the centrelines of all cylindrical sections and bifurcation modules lie on a single plane (the “meridional plane”), the internal flow passages are three-dimensional and complex and vary in a complex manner in the flow direction (see Figure 1 for a few examples). So a three-dimensional computational fluid dynamics (CFD) simulation is necessary to determine the fluid flow field.

For the out-of-plane configuration, the dimensions of the cylindrical sections and the bifurcation modules are the same as those of the in-plane configuration, but they are connected differently using a space-filling algorithm described below. For a comprehensible description of the complex three-dimensional arrangement, consider the orientations of various overlapping units of the network, each unit comprising a bifurcation module, a preceding mother branch, and two succeeding daughter branches—all of which must have centrelines lying on a single plane. For a particular unit U_n , suppose this plane is denoted by A_n . Now, consider a succeeding unit $U_{n+1,1}$ for which one of the daughter branches of unit U_n acts as the mother branch, followed by a bifurcation module and two daughter branches of its own. Similarly, one can think of another unit $U_{n+1,2}$, considering the second daughter branch of U_n . An important premise of the space-filling algorithm is that both the planes in which $U_{n+1,1}$ and $U_{n+1,2}$ lie are at right angle to plane A_n , while maintaining the bifurcation angle between themselves. The three-dimensional network may be better appreciated when a pictorial representation is included later in Section III B.

It is important to realize that apparent symmetry in the geometry of any two branches does not automatically imply symmetry in the flow field in those two branches. The combined effects of flow path curvature in the bifurcation module, flow division at a bifurcation, and inertia of the flow result in skewed velocity profiles (with maximum velocity near the inner edge of bifurcation) in the daughter branches even when the velocity field in the mother branch is symmetric about the bifurcation ridge between that mother and its daughter branches. Viscous effects try to establish a circumferentially symmetric paraboloid velocity profile in the straight portion of a branch but usually its length is insufficient for the complete removal of asymmetry, and the flow encounters the next bifurcation module where further asymmetry is introduced. Thus, even though each bifurcation appears to divide into two geometrically similar branches, the flow distribution is non-uniform.

The present numerical study attempts to capture the complex fluid dynamics associated with the above-mentioned three-dimensional branching networks. For each of the in-plane and out-of-plane configurations, three sets of computations are performed for bronchial networks comprising

TABLE I. Dimensions for the first six generations of the human bronchial tree according to Weibel.⁴

Generation number	Diameter (mm)	Length (mm)
G_0 (trachea)	18.00	120.00
G_1	12.20	47.60
G_2	8.30	19.00
G_3	5.60	7.60
G_4	4.50	12.70
G_5	3.50	10.70

generations G0-G3, G0-G4, and G0-G5, respectively. This is done so as to develop a systematic physical understanding of the generic fluid dynamic principles and features when a flow is divided in successive generations and the influence of the in-plane or out-of-plane construction of the network on the fluid dynamics. The separate simulations for G0-G3, G0-G4, and G0-G5 networks are undertaken so as to ascertain the effect of the extent of the branching network under consideration on the computed flow solutions in any particular branch. With the help of velocity contours, pressure contours, and distribution of mass flow in each branch, a qualitative and quantitative study is performed on the nature and evolution of flow asymmetry. It is shown that, although mass-flow asymmetry grows in each successive generation, there also exists a systematic order such that it is possible to ascertain the flow field in all branches of a particular generation by determining the flow field in some systematically selected branches of that generation, indicating a possible route to the saving of computational resource and time.

II. MATHEMATICAL FORMULATION AND SOLUTION METHODOLOGY

The present analysis considers steady, laminar, three-dimensional flow of a viscous and incompressible fluid through branching networks comprising generations G0-G3, G0-G4, and G0-G5 of a symmetrical model of the human bronchial tree. The in-plane and out-of-plane geometries are described in Section I. The corresponding three-dimensional models for the branching networks are built in SolidWorks 2010,²³ and the meshing and numerical simulations are performed on the ANSYS Workbench using the ANSYS Mesh Modeler and FLUENT,²⁴ respectively. All computations are performed on a Dell Optiplex 9010 with i5-3470 processor and 20 GB RAM.

A. Mathematical formulation

The steady incompressible flow in the complex branching networks is governed by the following generic conservation equations for mass and momentum:

Mass conservation:

$$\nabla \cdot \vec{v} = 0, \quad (1)$$

Momentum conservation:

$$\rho(\vec{v} \cdot \nabla)\vec{v} = -\nabla p + \nabla \cdot (\bar{\bar{\tau}}). \quad (2)$$

Here, \vec{v} represents the velocity vector of the fluid, ρ is the fluid density, p is the static pressure, and $\bar{\bar{\tau}}$ is the stress tensor given by the expression $\bar{\bar{\tau}} = \mu[\nabla\vec{v} + \nabla\vec{v}^T]$. Here, μ is the dynamic viscosity of the fluid. In the present study, the effect of gravitational force is neglected and external body forces are absent. In the present set of simulations, ρ and μ are taken as 1.225 kg/m^3 and $1.7894 \times 10^{-5} \text{ kg/ms}$, respectively.

A uniform velocity has been specified at the inlet to the bronchial tree, using the “Velocity Inlet” boundary condition feature of FLUENT. (Additional CFD simulations with paraboloid velocity profiles at inlet showed that the fluid flow field in downstream branches is not significantly altered.) The no-slip condition has been applied on the walls of the bronchial tubes. Since the present study considers only a segment of the bronchial tree, the conditions at the ends of the last generation branches are not known *a priori* (i.e., before the CFD simulations are run). Though textbooks on human physiology²⁵ present data pertaining to the pressure conditions in the alveolar regions where gaseous exchange takes place, there is a dearth of knowledge regarding the pressures at the intermediate branches of the bronchial tree. Hence, previous researchers^{7,8,14–18} have taken recourse to a pressure boundary condition at the ends of the last generation branches of the considered network. The same method is followed here by adopting the “Pressure Outlet” boundary condition feature of FLUENT²⁶ in which the static (gauge) pressure is specified at the outlet boundary. The values of all other flow quantities at the boundary are extrapolated from the interior by the “Pressure Outlet” feature. In our simulations, the gauge pressure in the “Pressure Outlet” panel has

been set to zero at all the outlets. The pressure throughout the computational domain is calculated with respect to this specified reference value at outlets, the attention being placed on the difference in static pressure at any location and that at outlets.

Specifying the velocity at inlet and the static pressure at outlet constitutes a well-posed problem for the CFD simulations. The “Velocity Inlet” feature of FLUENT does not fix the total properties of the flow. Therefore, the static pressure at the inlet is able to rise to whatever value that is needed to maintain the change of static pressure from inlet to outlet. The CFD simulations thus determine this change in static pressure between the inlet and outlet of the network (Δp_{io}). It is assumed that, for incompressible flow, this difference in static pressure (Δp_{io}) remains invariant (i.e., it is a function of the geometry of the network, Reynolds number, etc., but not of the absolute value of static pressure specified at the outlet). Accordingly, once the pressure difference between the inlet and any location in the network is determined from the CFD simulation, the absolute value of static pressure at that location can be calculated from the known value of static pressure at the inlet. If the static pressure is atmospheric at the inlet, then the actual gauge pressure at the outlet is negative. This negative gauge pressure inside the bronchial tree is responsible for driving air from the surroundings into the lungs.

The Reynolds number (Re) at the inlet to the trachea (generation G0) is an important parameter in this type of flows through bifurcating networks. An adult human typically breathes in about 6 l/min (considering a breathing rate of 12 with a tidal volume of 0.5 l) of air during normal conditions.^{3,27} The airflow in the upper airways usually remains laminar during normal breathing conditions. In the present simulations, which consider only laminar flow in the bifurcating networks, the Reynolds number at the inlet to generation G0 ($Re = 2\rho UR_{trachea}/\mu$) is varied from 400 to 1600 by varying the value of the velocity at the inlet (U).

B. Mesh generation

The bronchial tree network comprises tubes of gradually decreasing diameters and lengths. Thus, a multi-block meshing technique is used with gradually decreasing mesh sizes from the trachea to the lower generations. An unstructured mesh with sufficiently large number of elements²² is used in the present study. The surfaces of the branches have unstructured triangular elements while the volume contains tetrahedral elements. Inflation layers (O-grids) are used near the solid walls with sufficiently small thickness of the first layer, to capture the boundary layers accurately. The number of inflation layers is selected such that the height of the last layer is comparable to the size of the adjoining triangular face mesh.

C. Numerical method

The fluid flow equations (Equations (1) and (2)) are solved numerically using a commercial finite-volume based CFD package FLUENT.²⁴ The pressure-based solver available in FLUENT is used here. All transport equations are discretized to be at least second order accurate in space. The diffusion terms are discretized using the central difference scheme. When the main flow crosses the control volume boundaries obliquely, a second order upwind scheme should be used for the advection terms, to reduce numerical diffusion.²⁶ Since in an unstructured three-dimensional mesh (used here), the main flow is expected to cross the control volume boundaries obliquely, a second order upwind scheme is used here to discretize the advection terms in the governing transport equations. The following formulation is used by FLUENT to implement the second order upwind scheme:²⁶

$$\phi_f = \phi + \nabla\phi \cdot \vec{r}. \quad (3)$$

Here, ϕ and $\nabla\phi$ are, respectively, the cell-centred value of the flow variable and its gradient in the upstream cell. \vec{r} represents the displacement vector from the upstream cell centroid to the face centroid. The subscript “ f ” refers to the face centroid. The expression for $\nabla\phi$ may be found in Ref. 28. A segregated implicit solver is used to solve the resulting system of discretized equations. The SIMPLE algorithm with under-relaxation is employed in coupling the velocity and pressure

for solving the flow equations. In all simulations, a solution is said to be converged if the scaled residuals reach 10^{-8} for both the momentum and the continuity equations.

D. Grid independence study

In order to establish grid independence of the numerical solution, successive refinements of the unstructured mesh is considered. For each refinement, grid convergence is evaluated using a relative error measure (ε) of velocity magnitude (\bar{v}) between the coarse and fine solutions,

$$\varepsilon = \left| \frac{\bar{v}_{i, coarse} - \bar{v}_{i, fine}}{\bar{v}_{i, fine}} \right|. \quad (4)$$

The root-mean-square value of the relative error (ε_{rms}), which is calculated over a sufficiently large number of points (i), is used to provide a scalar measure of grid convergence for the points considered. Ideally, grid refinement studies should be based on refining the grid by a factor of 2 (grid halving). However, this is not a trivial task for a three dimensional unstructured mesh. The ε_{rms} values are a function of the grid refinement factor r_{grid} , and the order of discretization method applied q . To extrapolate ε_{rms} values to conditions consistent with true grid halving, the grid convergence index (GCI) has been suggested by Roache.²⁹ This method, based on Richardson extrapolation, can be applied for the fine grid solution as

$$GCI_{fine} = F_s \frac{\varepsilon_{rms}}{r_{grid}^q - 1}. \quad (5)$$

Based on a second-order discretization of all terms in space, q is equal to 2 for the present study. The value of r_{grid} is found from

$$r_{grid} = \left(\frac{N_{fine}}{N_{coarse}} \right)^{1/3}. \quad (6)$$

Here, N is the number of mesh elements. The factor of safety F_s , has been selected to be 3 to provide a GCI value equal to the ε_{rms} value when $r_{grid} = 2$ and $q = 2$. Therefore, the GCI value represents a scaled version of ε_{rms} , which accounts for mesh refinement factors less than 2. The two values each of ε_{rms} and r_{grid} , for the two sets of three meshes (coarse, medium and fine or medium, fine and very fine) used for establishing grid independence, are used to iteratively find a value of q . The closer the value of q comes to its original value (two), better is the grid independence.

The details of the meshes with results of the grid independence test for the in-plane configuration of the symmetric bronchial tree model are tabulated in Table II. Four meshes are used to establish grid independent solution: a coarse mesh comprising 372 418 elements, a medium mesh comprising 1 264 841 elements, a fine mesh comprising 4 798 473 elements, and a very fine mesh comprising 16 865 086 elements. The velocities and their gradients at the walls are found to be most sensitive to the mesh used in the calculations. Hence, the velocity magnitudes on various planes are used to establish grid independence of the solutions. The value of q is calculated to be 2.06 for the two sets of three meshes (coarse, medium and fine or medium, fine and very fine). Considering the grid independence data presented in Table II, the fine mesh is used for all subsequent simulations.

A similar procedure has been followed for establishing the grid independence of the solutions for the out-of-plane model as well. Four meshes are used to establish grid independent solution: a

TABLE II. Details of the grid independence study for the in-plane configuration of branching network comprising generations G0-G4 performed at $Re = 1600$.

Number of elements in mesh	r_{grid}	ε_{rms}	GCI
372 418 (coarse) - 1 264 841 (medium)	1.503	0.049	0.116
1 264 841 (medium) - 4 798 473 (fine)	1.560	0.018	0.037
4 798 473 (fine) - 16 865 086 (very fine)	1.520	0.013	0.030

TABLE III. Details of the grid independence study for the out-of-plane configuration of branching network comprising generations G0-G4 performed at $Re = 1600$.

Number of elements in mesh	r_{grid}	ϵ_{rms}	GCI
368 753 (coarse) - 247 826 (medium)	1.503	0.045	0.109
1 247 826 (medium) - 4 655 882 (fine)	1.551	0.023	0.050
4 655 882 (fine) - 16 563 184 (very fine)	1.527	0.020	0.042

coarse mesh comprising 368 753 elements, a medium mesh comprising 1 247 826 elements, a fine mesh comprising 4 655 882 elements, and a very fine mesh comprising 16 563 184 elements. The value of q is calculated to be 1.96 for the two sets of three meshes (coarse, medium and fine or medium, fine and very fine). Considering the grid independence data presented in Table III, the fine mesh is used for all subsequent simulations.

E. Validation of results

The present numerical method was validated by applying it to the flow through a single bifurcation unit.^{10,11} Zhao and Lieber¹⁰ measured steady inhalation airflow through a symmetric single bifurcation airway. Measurements of the velocity in the bifurcation plane (defined as the plane containing the centrelines of the mother and daughter branches in Ref. 10) and transverse planes (normal to the bifurcation plane) were carried out at three different values of inlet Reynolds number (i.e., $Re = 518$, 1036, and 2089) and 17 different locations in the complete geometry. The geometry of Zhao and Lieber¹⁰ is reproduced here, and the velocity profile in the bifurcation plane is compared (Figure 2). In the same figure, the numerical results of Comer *et al.*³⁰ are also included, to show the difference in numerical and experimental results that may be partly attributed to experimental uncertainties. All velocities are presented on a plane at the junction of the bifurcation module and the cylindrical section of the left daughter branch. The numerical results are symmetric about the centreline of the mother branch and hence the velocities on the right branch are not shown here. Zhao and Lieber¹⁰ had reported slight asymmetries in the flow in the two daughter branches and this may also be responsible for the deviation of the numerical results from their measurements. The present results agree well with the experimental measurements of Zhao and Lieber,¹⁰ as seen in Figure 2. The agreement of the present computations with the experimental results near the

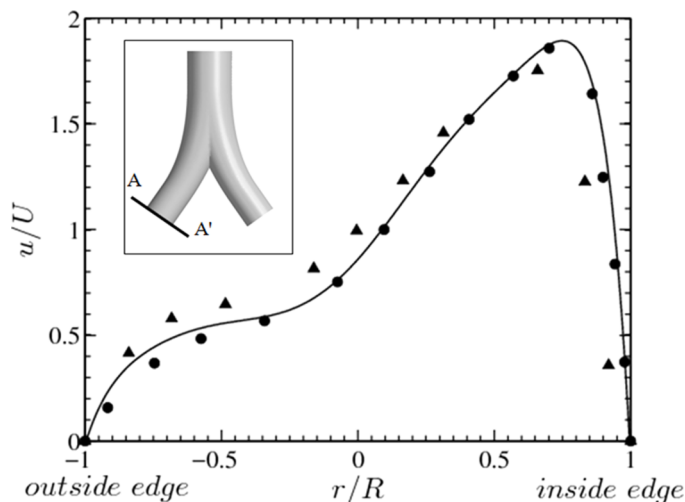


FIG. 2. Comparison of the axial velocity profile in the meridional plane at the outlet of the left daughter branch (line A-A') in a single bifurcation geometry for $Re = 1036$. \blacktriangle Experimental,¹⁰ \bullet Numerical,³⁰ — Numerical (present solution).

outside edge (toward point A of the figure in inset) is superior to the numerical results of Comer *et al.*³⁰ Similar good agreements of the present results and the experiments are found at other Reynolds numbers and other locations of measurement not shown in Figure 2. This establishes the capability of the present numerical method in accurately capturing the complex fluid dynamics in three-dimensional multi-generation bronchial networks.

III. NOMENCLATURE FOR THE BRANCHING NETWORK

A systematic nomenclature of the various branches and planes in the complex three-dimensional branching networks is important for a comprehensive understanding of the prevalent fluid dynamics. This section illustrates the naming system developed for both the in-plane and out-of-plane configurations. The nomenclature is presented for the branching network G0-G5, and the same systematic naming is also valid for the branching networks consisting of generations G0-G3 and G0-G4.

A. In-plane configuration

Figure 3 shows a three-dimensional view of the in-plane configuration of generations G0-G5 of branching networks (according to the dimensions given in Table I), along with the systematic naming of the branches and planes in the successive generations. As mentioned previously in Section I, this configuration of the branch network is constructed from cylindrical sections and bifurcation modules, all of which must have centrelines lying on a single plane (the meridional plane). All the branches are denoted by four characters “GnBk,” where “Gn” denotes the generation to which the branch belongs while “Bk” denotes the branch number in a particular generation. The branches of the same generation are numbered serially from left to right as shown in Figure 3. For example, the trachea which is the solitary branch in generation G0 is denoted by “G0B1”. The branch of generation G1 which lies to the left of the tracheal centreline is denoted by “G1B1” while that which lies to the right is denoted by “G1B2”.

The ends of the cylindrical sections of the various branches have also been systematically named for easy reference in the description of the flow features on the specified cross sections. The end-planes of the branches are denoted by “GnP_k”, where “Gn” denotes the generation to which the

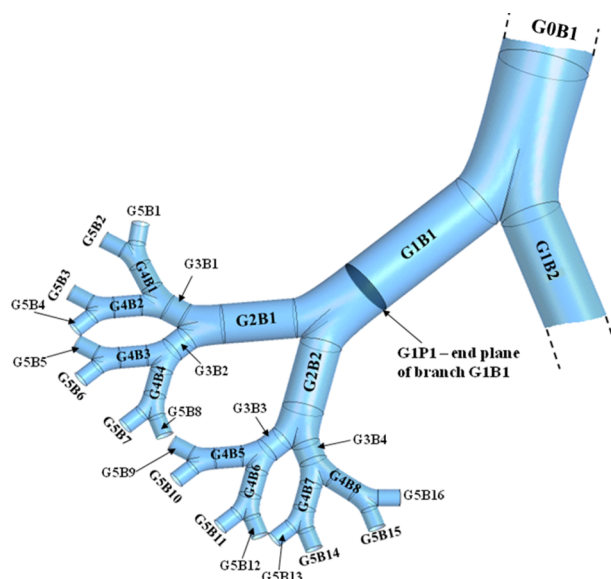


FIG. 3. Six generations (G0-G5) of a symmetric model of the human bronchial tree; in-plane configuration. [Only half of the network is shown for clarity; CFD simulations are run for the entire network.]

branch belongs and “ P_k ” denotes the end-plane of the branch “ B_k ”. As an example, the end-plane of branch “G1B1” is denoted by “G1P1” (this plane has been highlighted in Figure 3).

A “longitudinal symmetry plane” is defined in this paper as the plane that passes through the centreline of generation G0 and perpendicular to the plane that contains the centrelines of branches G0B1, G1B1 and G1B2.

B. Out-of-plane configuration

Figure 4 shows a three-dimensional view of the out-of-plane configuration of generations G0-G5 of branching networks (according to the dimensions given in Table I). As mentioned previously in Section I, this configuration of the branch network is also constructed from cylindrical sections and bifurcation modules, which are however, connected to each other in a different manner so as to form a space-filling three-dimensional structure. The same system is followed for naming the branches and cross-sectional planes in the out-of-plane configuration as in the case of the in-plane configuration. However, due to the complex three-dimensional arrangement of branches in the out-of-plane configuration (as explained in Section I), it is difficult to explain the nomenclature of the branches in the same generation. Figure 4 may be referred to for a better understanding of the system followed for naming the branches.

A “longitudinal symmetry plane” is defined in the same manner as in Section III A. In addition, for the out-of-plane configuration, a “transverse symmetry plane” is defined as the plane that contains the centrelines of branches G0B1, G1B1 and G1B2.

IV. RESULTS AND DISCUSSION

In any dichotomously branching network, the flow is forced to diverge as it encounters a bifurcation and two streams are completely separated after the fluid flows past the bifurcation ridge. The proportion of the total flow that is directed into each of the two daughter branches of the same mother branch is mainly governed by the flow distribution in the mother branch about a plane that contains the centreline of the mother branch and passes through the bifurcation ridge. So, as long as the contours of flow variables on a plane at the end of a particular branch are symmetric about the bifurcation ridge just downstream of it, the two daughter branches emanating from that

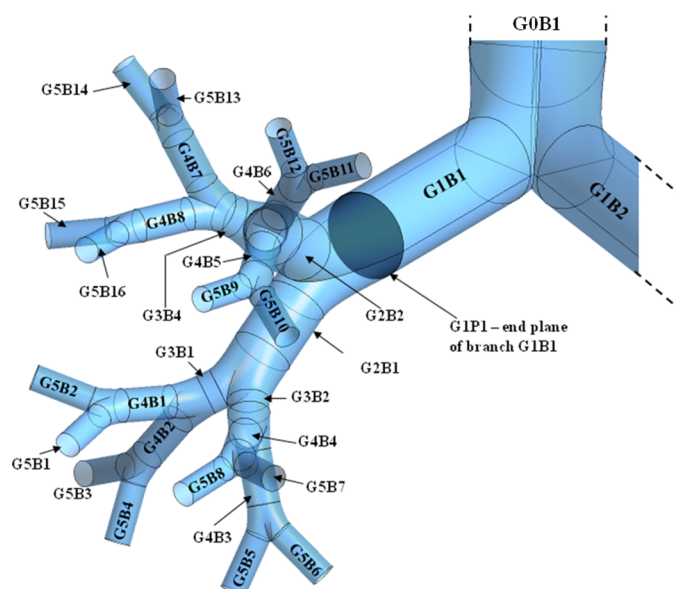


FIG. 4. Six generations (G0-G5) of a symmetric model of the human bronchial tree; out-of-plane configuration. [Only half of the network is shown for clarity; CFD simulations are run for the entire network.]

mother branch show similar flow features. This is why the flow characteristics with respect to the bifurcation ridges have been highlighted in the following discussion.

As part of the present series of investigation, simulations are performed for the range $400 \leq Re \leq 1600$, where Re is the Reynolds number at the inlet to the trachea. However, the principal thrust of the present paper is to develop a physical understanding of the fluid dynamics and its dependence on the configuration of the branching network (in-plane versus out-of-plane) and the extent of the network under consideration (four, five, or six generations). Therefore, the detailed quantitative results are presented here only at one representative value of the Reynolds number, viz., $Re = 1000$.

A. Four-generation network (G0-G3)

In this section, the flow characteristics in four generations (G0-G3) of branching network according to the dimensions given in Table I are investigated. The contours of velocity magnitude are plotted at strategic locations to determine how the flow divides as it travels down successive bifurcations. The representational convention for the cross sections has been adopted such that the main flow is towards the reader.

1. In-plane configuration (G0-G3)

The contours of velocity magnitude on the planes G0P1, G1P1 and G1P2 are shown in Figure 5. Traces of the respective downstream bifurcation ridges are superimposed on each of the contours since the symmetry (or asymmetry) of the flow field with respect to these lines influences how the flow would get divided at the downstream bifurcation. At the end of the cylindrical section of generation G0 (i.e., at plane G0P1), the velocity contour is represented by concentric circles of gradually increasing magnitudes from zero at the wall to maximum at the centre of the cross section. This is typically the velocity distribution in the developing region of a circular pipe. As the length of the cylindrical section is less than that required for the flow to become fully developed, the maximum velocity at the centre (~ 1.2 m/s) is smaller than 1.62 m/s which is twice the average velocity for $Re = 1000$ (i.e., fully paraboloid velocity distribution characteristic of laminar fully developed flow is not yet obtained). Owing to the symmetry of the velocity distribution on plane G0P1 about the bifurcation ridge, the two daughter branches (G1B1 and G1B2) receive the same flow from the mother and show similar flow features. As the flow from the trachea is divided into two streams, one turns left to enter branch G1B1 and the other turns right to enter branch G1B2. Therefore, the velocity contours on planes G1P1 and G1P2 are mirror images of each other (as seen in Figure 5). Due to the combined effects of flow path curvature and inertia of the flow, the velocity contours on the planes G1P1 and G1P2 are asymmetric (about the bifurcation ridges just downstream of the planes) with the maximum velocity occurring towards the inner edge of the bifurcation (this is true for both branches). This asymmetry on planes G1P1 and G1P2 with respect to the downstream bifurcation ridges results in dissimilar flow distribution among the branches of generation G2.

Figure 6 shows the contours of velocity magnitude on the planes G2P1 and G2P2. The velocity contour on plane G1P1 is also reproduced in Figure 6 for the ease of connecting flow features in G2 with upstream flow history. Due to the effects of flow path curvature, the location of the maximum velocity in either of the two branches G2B1 and G2B2 is shifted towards the central axis of the bifurcation module (between G1B1 and its two daughter branches) as compared to the locations in the corresponding halves of plane G1P1. However, the asymmetry in the velocity contour on plane G1P1 about its downstream bifurcation ridge results in two dissimilar flows entering the branches G2B1 and G2B2. As the velocity magnitude on plane G1P1 was higher on the inner side of the preceding bifurcation module, the maximum (and also average) velocity on plane G2P2 is greater than that on plane G2P1. A careful observation of the velocity contour on plane G2P1 shows that if the velocity is plotted along any line which is horizontal in the diagram there exist two peaks (maxima): one near the centre of the cross section and the other towards the inner edge of the

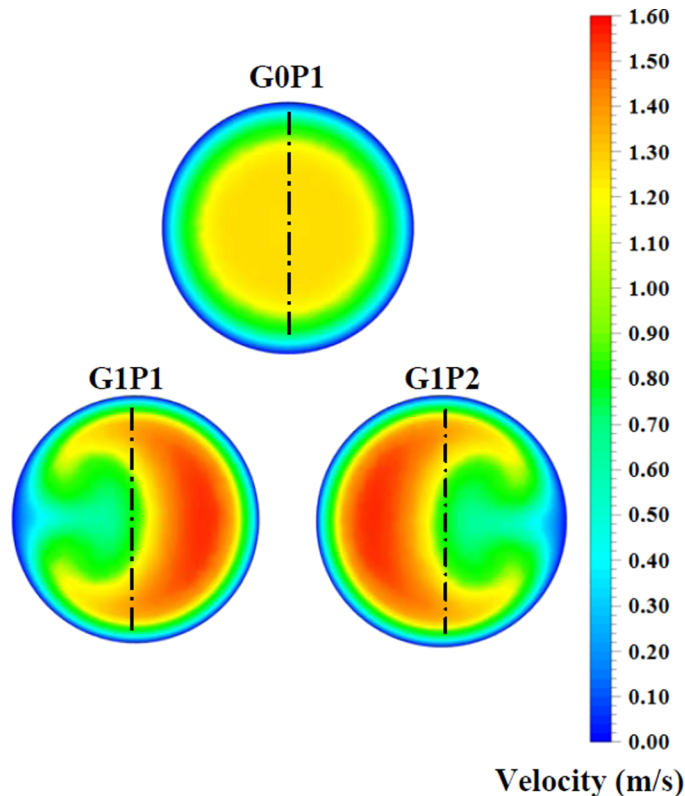


FIG. 5. The velocity contours on the cross-sectional planes at the end of the cylindrical sections of the branches of generations G0 and G1 in a four-generation branching network; in-plane configuration. — · — Traces of the respective downstream bifurcation ridges.

preceding bifurcation (see Figure 1 for the definition of inner edge). The velocity distribution along any horizontal line on plane G2P2, on the other hand, shows only one maxima as one moves from wall to wall. Hence, the flow features in branch G2B1 are considerably different from that in branch G2B2.

Although the velocity contours on the planes G1P1, G1P2, G2P1 and G2P2 are all asymmetric about their downstream bifurcation ridges, a horizontal line can be constructed for each plane, passing through the centres of the cross sections, that divides the velocity contours into two symmetric parts. In general, for the in-plane configuration, the flow solution on any cross-sectional plane is symmetric with respect to the centreline which is formed through the intersection of the cross-sectional plane and the meridional plane.

Since the velocity contour on plane G1P2 is a mirror image of that on plane G1P1 (Figure 5), it can be inferred (which is also confirmed by computed values) that the flow features in the branching network originating from G1B2 are similar to those in the branching network originating from G1B1. Conversely, since the velocity contours on planes G2P1 and G2P2 have no visible similarity between themselves, the flows in the branches G3B1, G3B2, G3B3 and G3B4 are all different from one another. Similarly, the flow field in the branches G3B5, G3B6, G3B7 and G3B8 are all different from one another.

In Figure 7, the mass flow rates in the eight branches of generation G3 are shown for $Re = 1000$. Previously (in Figure 5) it was established that the flows in the branches G1B1 and G1B2 are equal. However, as one proceeds further downstream, the flow field becomes asymmetric (about the bifurcation ridge) and consequently, the mass flow rates in the branches G2B1 and G2B2, emanating from branch G1B1, are unequal. Similarly, the mass flow rates in the branches G2B3 and G2B4, emanating from branch G1B2, are also unequal. In spite of this unequal mass-flow distribution among the branches emerging from the same mother branch, symmetry in the flow

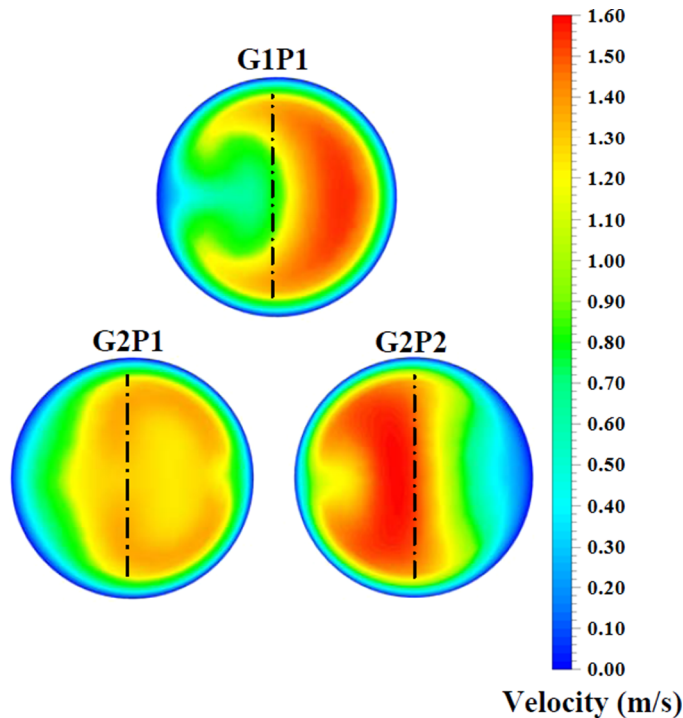


FIG. 6. The velocity contours on the cross-sectional planes at the end of the cylindrical sections of selected branches of generations G1 and G2 in a four-generation branching network; in-plane configuration. — · — Traces of the respective downstream bifurcation ridges.

distribution is visible among the pairs of branches G2B1-G2B4 and G2B2-G2B3 owing to the symmetry of mass flow in branches G1B1 and G1B2. Such flow distribution features are transmitted downstream and as a consequence, symmetry prevails among the pairs of branches G3B1-G3B8, G3B2-G3B7, G3B3-G3B6, and G3B4-G3B5. So, knowledge about the asymmetric mass-flow distribution through branches G3B1, G3B2, G3B3 and G3B4 is necessary and sufficient for describing the flow at generation G3.

Figure 7 shows that the mass flow rate in branch G3B3 (or G3B6) is the greatest among that in all the G3 branches originating from branch G1B1 (or G3B1). This is attributable to the combined effects of flow path curvature and inertia of the flow. As the fluid flows through the bifurcation module joining branches G0B1, G1B1 and G1B2, the flow path curvature drives greater mass of fluid towards the central axis of the bifurcation module. The insufficient length of the G1 branches prevents the viscous effects from establishing symmetric paraboloid velocity profile at the entrance to the bifurcation modules connecting the branches of generations G1 and G2. Consequently, greater mass of fluid flows through that portion of branch G1B1 (or G1B2) from where the flow is directed into branch G2B2 (or G2B3). Hence, the flow rates through branches G2B2 and G2B3 are considerably greater than those through branches G2B1 and G2B4. Similar effects of flow path curvature in the bifurcation modules connecting the branches of generations G2 and G3, together with the small lengths of the G2 branches, result in the maximum flow rate in G3B3 (and G3B6), and the minimum flow rate in G3B1 (and G3B8).

From the above discussion, one can make the following two generalizations for the in-plane configuration. (i) In order to ascertain the flow field in the complete network, it is necessary and sufficient to obtain the flow field in the branches on one side of the plane (denoted as “longitudinal symmetry plane” in this paper) passing through the centreline of generation G0 and perpendicular to the meridional plane. (ii) From generation G2 onwards, the flow fields in the various branches of the same generation lying on any one side of the longitudinal symmetry plane are all different.

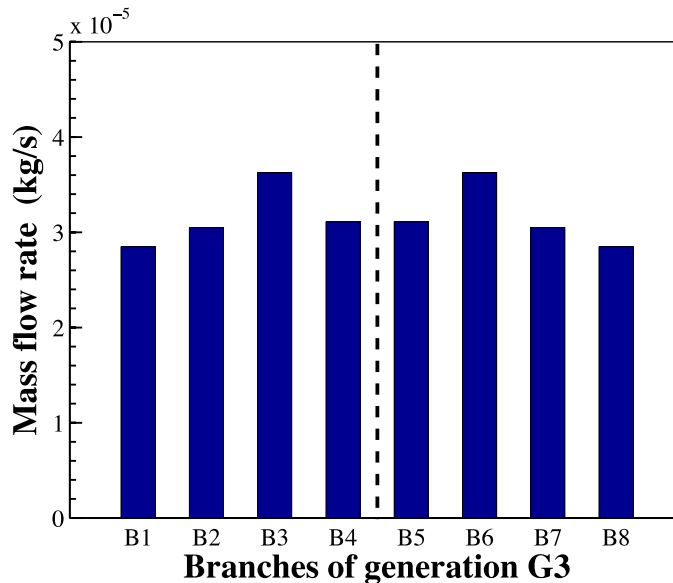


FIG. 7. The asymmetric mass-flow distribution in the branches of generation G3 in a four-generation branching network; in-plane configuration. --- Schematic depiction of the longitudinal symmetry plane dividing the geometry into two parts showing similar flow features.

2. Out-of-plane configuration (G0-G3)

The contours of velocity magnitude on the planes G0P1, G1P1 and G1P2 in the out-of-plane configuration are shown in Figure 8. Traces of the respective downstream bifurcation ridges are superimposed on each of the contours since the symmetry (or asymmetry) of the flow field with respect to these lines influences how the flow would get divided at the downstream bifurcation. The contours on the planes G0P1, G1P1 and G1P2 in the out-of-plane configuration are observed to be similar to those on the same planes in the in-plane configuration (Figure 5). This is because the flow follows exactly the same path for both the configurations till the planes G1P1 and G1P2; however, differences in the velocity contours in the two configurations, downstream of these planes, arise due to the rotation of the downstream bifurcation ridge through 90° (due to reasons explained in Section I). The superimposed traces of the downstream bifurcation ridges for the planes G1P1 and G1P2 are horizontal lines (Figure 8) instead of vertical lines as found for the in-plane configuration (Figure 5). As a result, the velocity contours on planes G1P1 and G1P2 are not only mirror images of one another but are also symmetric about the downstream bifurcation ridge. Hence, although the flow entering the branches G2B1 and G2B2 in the in-plane configuration was different from each other, in the out-of-plane configuration, the flow features in branches G2B1 and G2B2 are mirror images of each other. This is borne out by the computed results shown in Figure 9. A comparison of Figures 9 and 6 shows clearly how the flow in generation G2 is affected fundamentally as a result of configurationally different arrangement of the same flow modules.

The velocity contours on plane G1P1 as shown in Figure 9 are the same as those in Figure 8 but the cross section is rotated by 90° . This is according to a representational convention adopted here such that, for any bifurcation module involving a mother branch and two daughter branches, the trace of the bifurcation ridge appears vertical on the cross-sectional plane of the mother branch and the primary flow is directed towards the reader. This adopted convention makes it easier to identify symmetry in the flow field in the complex three-dimensional arrangements of the cross sections of various branches.

Figure 10 shows the contours of velocity magnitude on planes G3P1, G3P2, G3P3 and G3P4. The velocity contours on planes G2P1 and G2P2 are also reproduced in Figure 10 for the ease of connecting flow features in G3 with upstream flow history. The velocity contours on planes G2P1 and G2P2 as shown in Figure 10 are the same as those in Figure 9 but the cross sections are rotated

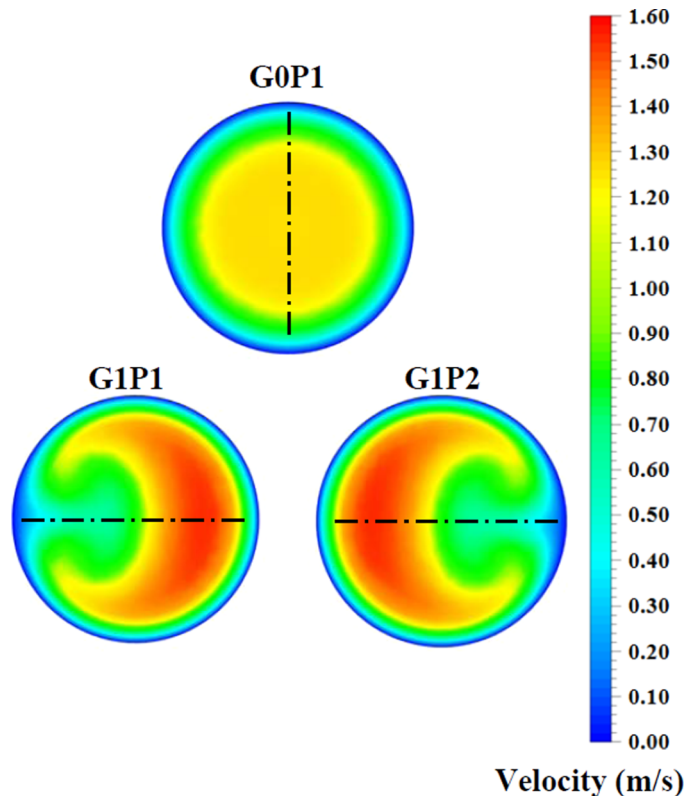


FIG. 8. The velocity contours on the cross-sectional planes at the end of the cylindrical sections of the branches of generations G0 and G1 in a four-generation branching network; out-of-plane configuration. — · — Traces of the respective downstream bifurcation ridges.

by 90° , in accordance with the representational convention adopted here. The velocity contour on plane G2P1 is asymmetric about the downstream bifurcation ridge. As a result, the flow patterns in the daughter branches of branch G2B1 (viz., branches G3B1 and G3B2) are different from one another. Hence, the velocity contours on planes G3P1 and G3P2 are different from one another. As the velocity magnitude on plane G2P1 was higher on the inner side of the preceding bifurcation module, the maximum (and also average) velocity on plane G3P2 is greater than that on plane G3P1. Moreover, the velocity contour on plane G2P2 is just the mirror image of that on plane G2P1. Hence, the flow patterns in the branches G3B3 and G3B4 are also the mirror images of those in the branches G3B2 and G3B1, respectively.

It is inferred from Figures 9 and 10 that for the out-of-plane configuration, the velocity field is not only symmetric about the longitudinal symmetry plane but also about the transverse symmetry plane (defined in Section III B) which contains the centrelines of the branches G0B1, G1B1 and G1B2. However, the symmetry in the flow field (with respect to a centreline) that was observed on any cross-sectional plane in the in-plane configuration is lost from generation G2 onward for the out-of-plane configuration.

Figure 11 shows the mass flow rates in the eight branches of generation G3 for the out-of-plane configuration at $Re = 1000$. Since the flow-path in the out-of-plane configuration is the same as that in the in-plane configuration up to the end of generation G1, the mass-flow distribution is also identical in both the configurations up to generation G1. However, due to the rotation of successive flow units (as defined in Section I) by 90° in the out-of-plane configuration, the velocity on plane G1B1 is symmetric about the downstream bifurcation ridge (as shown in Figure 9). Consequently, the flow rates in the branches G2B1 and G2B2 are equal. Moreover, due to the equality of mass flow rates in branches G1B1 and G1B2, the flow rates in branches G2B3 and G2B4 are equal to those in

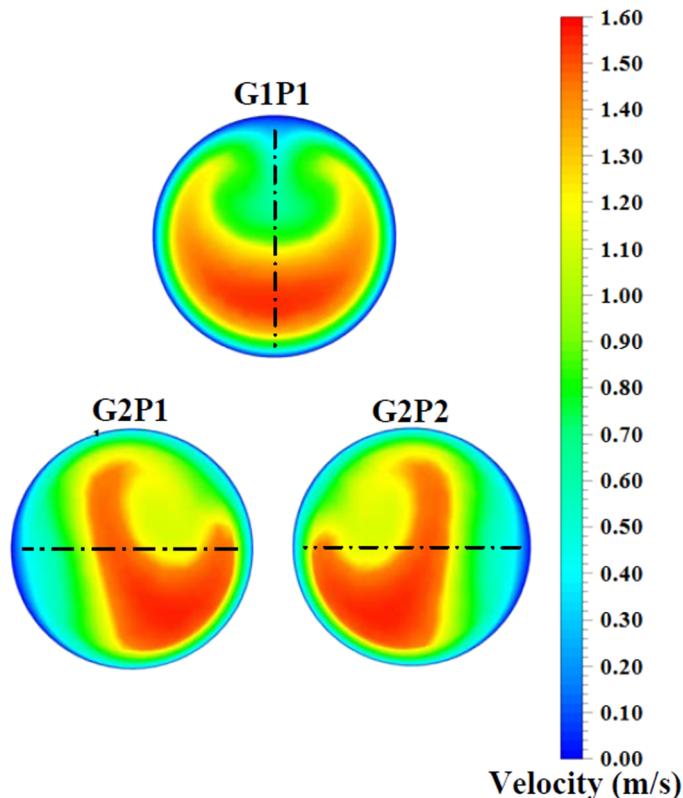


FIG. 9. The velocity contours on the cross-sectional planes at the end of the cylindrical sections of selected branches of generations G1 and G2 in a four-generation branching network; out-of-plane configuration. — · — Traces of the respective downstream bifurcation ridges.

G2B2 and G2B1, respectively. Therefore, the flow rates in all the G2 branches of the out-of-plane configuration are equal.

It is shown in Figure 10 that the velocity contour on plane G2P1 is not symmetric about the downstream bifurcation ridge. Hence, the flow rates in branches G3B1 and G3B2 are unequal. However, since the velocity contours on planes G2P1 and G2P2 are mirror images of each other, the flow rates in branches G3B1 and G3B4 are equal, and those in branches G3B2 and G3B3 are also equal. Owing to the symmetry in the flow field, similar features are observed for the branches lying on the other side of the longitudinal symmetry plane (i.e., G3B5-G3B8). Therefore, Figure 11 shows that the non-uniform mass-flow distribution among the branches of generation G3 is such that the knowledge of the mass flowing through any two of them originating from the same mother branch (say, branches G3B1 and G3B2) is necessary and sufficient for determining the mass flow rate in all the other branches in generation G3.

An interesting effect of the configurationally different arrangement of the same flow modules is the change in the non-uniformity of the mass-flow distribution. The difference between the maximum and minimum mass flow rates in the branches of a particular generation gives an indication of the non-uniformity in the mass-flow distribution. It is observed from Figures 7 and 11 that the non-uniformity in the mass-flow distribution is much greater in the branches of generation G3 for the in-plane configuration as compared to that in the out-of-plane configuration.

From the above discussion, one can make the following generalizations for the out-of-plane configuration. (i) In order to ascertain the flow field in the complete network, it is necessary and sufficient to obtain the flow field in the branches in one of the four quarters of the three-dimensional branching network defined through the intersection of the longitudinal and transverse symmetry plane (defined in Section III B). (ii) From generation G2 onwards, the flow fields in the various branches of the same generation lying on any one side of the longitudinal symmetry plane are all

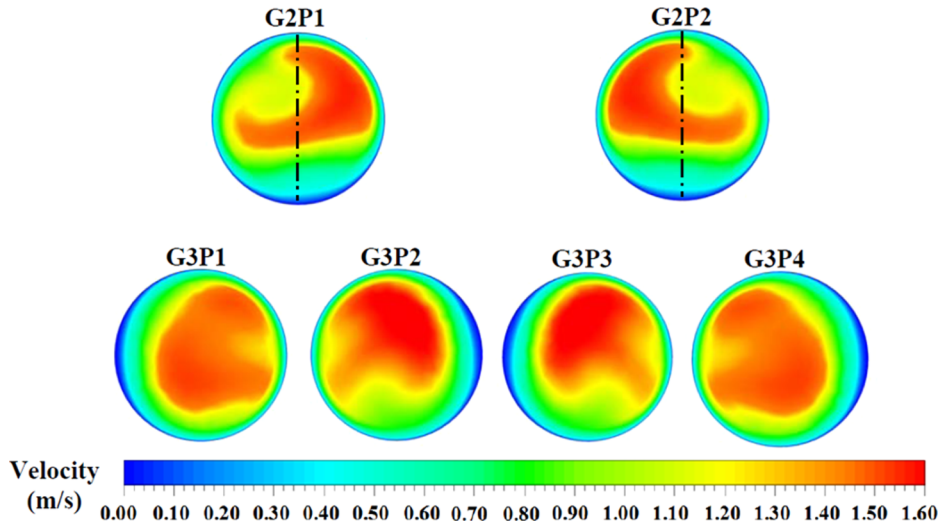


FIG. 10. The velocity contours on the cross-sectional planes at the end of the cylindrical sections of selected branches of generations G2 and G3 in a four-generation branching network; out-of-plane configuration. — · — Traces of the respective downstream bifurcation ridges.

symmetric about the transverse symmetry plane. (iii) From generation G3 onwards, the flow fields in the various branches of the same generation lying in any quarter defined through the intersection of the longitudinal symmetry plane and the transverse symmetry plane are all different. (iv) The non-uniformity in the mass-flow distribution is smaller for the out-of-plane configuration as compared to that for the in-plane configuration.

B. Five-generation network (G0-G4)

A detailed study was performed for four generations (G0-G3) of branching network in Sec. IV A, showing the symmetry (or lack of it) in the flow characteristics and the effects of configurationally different three-dimensional arrangement of the branches. In this section, the flow characteristics in five generations (G0-G4) of a branching network are investigated. Since the velocity field in generations G0-G3 of the five-generation network is observed to be similar to that in the four-generation network, this section discusses the variation of the gauge static pressure in the five-generation network which is found to be different from that in the four-generation network. The representational convention adopted for the pressure contours is the same as that used for the velocity contours in Section IV A.

1. In-plane configuration (G0-G4)

Figure 12 shows the contours of gauge static pressure on planes G1P1, G1P2, G2P1 and G2P2. Traces of the respective downstream bifurcation ridges are superimposed on each of the contours since the symmetry (or asymmetry) of the flow field with respect to these lines influences how the flow would get divided at the downstream bifurcation. The flow through the trachea divides into two equal streams at the bifurcation ridge downstream of plane G0P1. One stream turns left to enter branch G1B1 while the other turns right to enter branch G1B2. As a result, the pressure contours on planes G1P1 and G1P2 are mirror images of each other. Moreover, the pressure contours on these planes are symmetric about a horizontal (in the diagram) line passing through the centre of the plane. However, the pressure contours on the planes G1P1 and G1P2 are asymmetric about their downstream bifurcation ridges leading to dissimilar flow fields in their daughter branches. The contours on the planes G1P1 and G1P2 show that the maximum pressure occurs near the top and bottom walls, while two regions of low pressure develop near the centre.

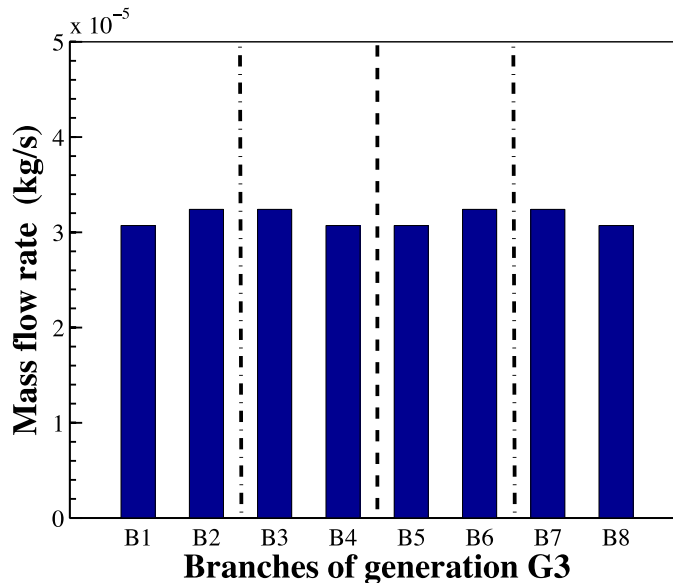


FIG. 11. The asymmetric mass-flow distribution in the branches of generation G3 in a four-generation branching network; out-of-plane configuration. --- Schematic depiction of the longitudinal symmetry plane dividing the geometry into two parts showing similar flow features. - · - Schematic depiction of the transverse symmetry plane which further divides the geometry resulting into four parts which possess similar flow features.

As the pressure contour on plane G1P1 is asymmetric about the downstream bifurcation ridge, the pressure contours on the planes G2P1 and G2P2 are different from one another. Figure 12 shows that the maximum (and average) static pressure on the plane G2P2 is much greater than that on plane G2P1. As in the case of planes G1P1 and G1P2, the contours on the planes G2P1 and G2P2 show maximum pressures occurring near the top and bottom walls. Although the pressure contours on planes G2P1 and G2P2 are asymmetric about their respective downstream bifurcation ridges, they are found to be symmetric about a horizontal (in the diagram) line passing through the centre of the plane.

Since the pressure contour on plane G1P2 is a mirror image of that on plane G1P1, it can be inferred (which is also confirmed by computed values) that the flow features in the branching network originating from branch G1B1 are similar to those originating from G1B2. Hence, the pressure contours on planes G3P8, G3P7, G3P6 and G3P5 are the mirror images of those on planes G3P1, G3P2, G3P3 and G3P4, respectively. Conversely, since the pressure contours on planes G2P1 and G2P2 have no visible similarity between themselves, the pressure contours on the planes G3P1, G3P2, G3P3 and G3P4 are all different from one another.

The mass-flow distribution among all the branches of the in-plane configuration in a five-generation network at $Re = 1000$ is shown in Figure 13. The solid vertical lines are drawn to distinguish different generations from G0 to G4. The distance between a solid line and the next dotted vertical line to its right represents the average mass flow rate per branch of that generation. The lengths of the horizontal bar graphs represent the mass flowing through a particular branch. For example, the two branches G1B1 and G1B2 have the same mass flow rates and therefore the lengths of the horizontal bars are equal (and the same as the average flow rate). It has already been shown that in spite of the asymmetry in the flow field, there exists a systematic order such that the flow distribution is symmetric about the longitudinal symmetry plane. Hence, a symmetry line (horizontal dashed line in Figure 13) may be constructed such that the mass-flow distribution on one side of it (say, the bottom side) is the mirror image of that on the other side. So, knowledge about the asymmetric mass-flow distribution in branches G4B1-G4B8 is necessary and sufficient for describing the flow at generation G4. The following discussion is therefore confined to the branches lying on one side of the constructed line.

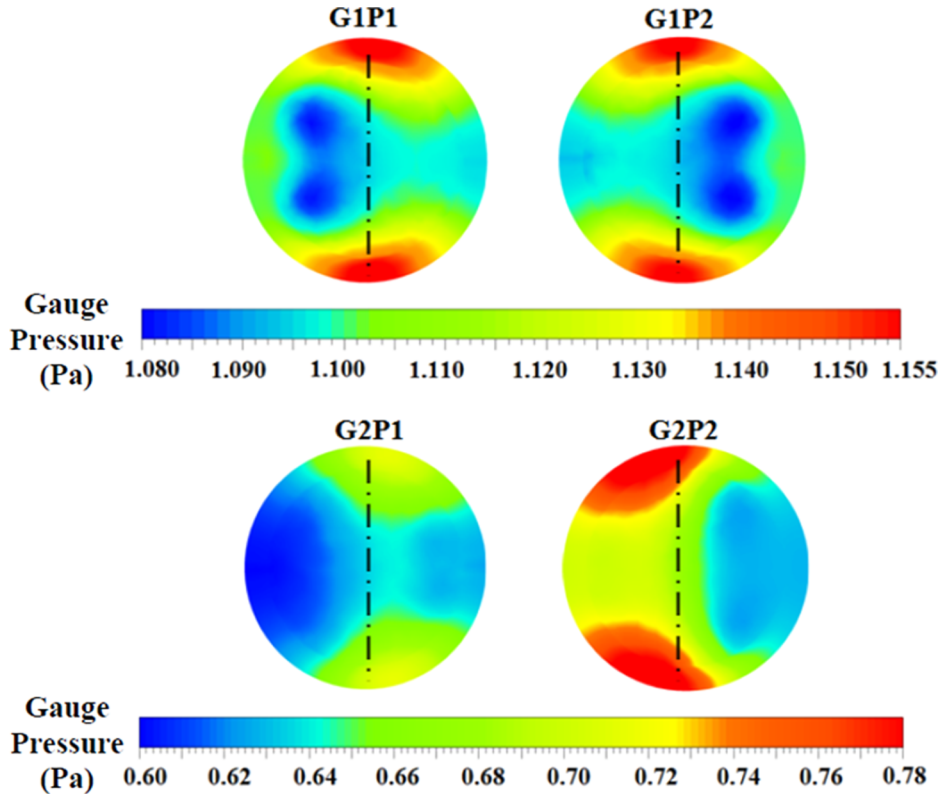


FIG. 12. Contours of gauge static pressure at the end-planes of selected branches of generations G1 and G2 in a five-generation branching network; in-plane configuration. — · — Traces of the downstream bifurcation ridges.

The asymmetry in mass-flow distribution is visible from generation G2 where the mass flow rate in G2B2 is different from that in G2B1. This asymmetry in flow distribution is propagated to the next generation (G3) and the flow rates in branches G3B1-G3B4 are all different. The maximum flow rate in generation G3 is found to occur in branch G3B3 while the minimum flow rate occurs in branch G3B1. Four of the eight G4 branches lying on one side of the longitudinal symmetry plane are found to have mass flow rates greater than the average flow rate in generation G4. The maximum flow rate in generation G4 is found in branch G4B6 while the minimum flow rate occurs in branch G4B1.

From the above discussion, it is inferred that the generalizations made for the four-generation network (Section IV A 1) hold true for the five-generation network as well. Moreover, for a n -generation branching network in the in-plane configuration, the determination of the asymmetric mass-flow distribution in 2^{n-2} branches of the n th generation (i.e., $G_n - 1$), lying on one side of the longitudinal symmetry plane, is necessary and sufficient to ascertain the mass-flow distribution in the complete network.

2. Out-of-plane configuration (G0-G4)

As mentioned previously, the flow-path in the out-of-plane configuration is identical to that in the in-plane configuration up to the planes G1P1 and G1P2. Hence, the pressure distributions on the above-mentioned planes are also similar to those shown in Figure 12. The following discussion is thus confined to cross-sectional planes in the branches lying on one side of the longitudinal symmetry plane (i.e., branches originating from G1B1). As in the case of the velocity contours in the out-of-plane configuration of the four-generation network (Figure 9), the pressure contour on the plane G1P1 turns out to be symmetric about its downstream bifurcation ridge due to the 90° rotation of successive flow units. Consequently, the pressure contours on planes G2P1 and G2P2

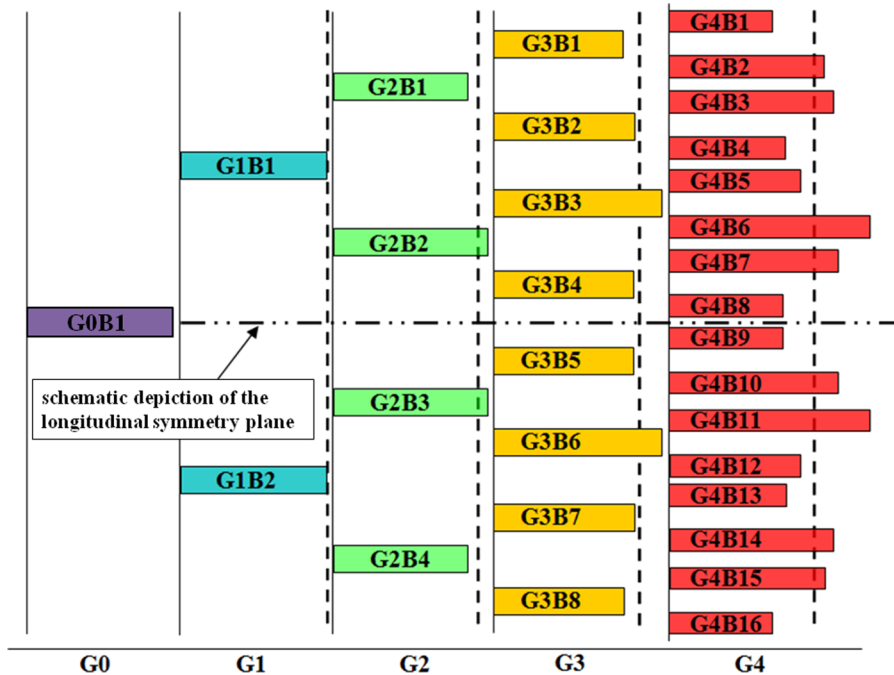


FIG. 13. Mass flow rates in all the branches in a five-generation branching network; in-plane configuration. [The horizontal distance between a solid vertical line (representing the start of a generation) and the following dashed line indicates the average mass flow rate per branch in the generation.]

are mirror images of one another (Figure 14). This is in contrast to the dissimilar pressure contours on planes G2P1 and G2P2 for the in-plane configuration (Figure 12). Moreover, symmetry about the longitudinal symmetry plane ensures that the pressure contours on planes G2P3 and G2P4 are mirror images of those on G2P2 and G2P1, respectively. It is thus possible to predict the pressure field in all the branches of generation G2 of the out-of-plane configuration from that in any one of them.

The contours of gauge static pressure on the end-planes of the branches of generations G3 are also shown in Figure 14. Since the pressure contour on plane G2P1 is not symmetric about the downstream bifurcation ridge, the pressure contours on the planes G3P1 and G3P2 are different from each other. Similarly, the pressure contours on planes G3P3 and G3P4 are also dissimilar. In spite of this asymmetry among the G3 branches, the pressure contours on planes G3P1 and G3P2 are mirror images of those on the planes G3P4 and G3P3, respectively, due to the similarity in the contours on plane G2P1 and G2P2. Therefore, in order to determine the pressure distribution in all the branches of generation G3, it is necessary and sufficient to obtain the pressure field in any one of the four branch pairs emerging from the four G2 branches. Similar trends extend to the G4 branches as well, and it is necessary and sufficient to determine the flow field in four G4 branches lying in a quarter of the network defined through the intersection of the longitudinal and transverse symmetry planes (i.e., four branches which have originated from the same G2 branch). Figure 14 also shows that from generation G2 onward for the out-of-plane configuration, there exist no cross-sectional centrelines about which the pressure contours are symmetric.

The mass flow rates in all the branches of the out-of-plane configuration in a five-generation network at $Re = 1000$ are shown in Figure 15. The same representational convention has been used here as in Figure 13. In contrast to the unequal mass flow rates through the branches of generation G2 in the in-plane configuration (Figure 13), the branches of generation G2 in the out-of-plane configuration (Figure 15) have equal mass flow rates. This allows the construction of two more lines of symmetry (as shown in Figure 15 by the horizontal dashed lines between branch pairs G2B1-G2B2 and G2B3-G2B4) in addition to the symmetry line in Figure 13. These two new lines schematically depict the transverse symmetry plane which exists for the out of plane configuration.

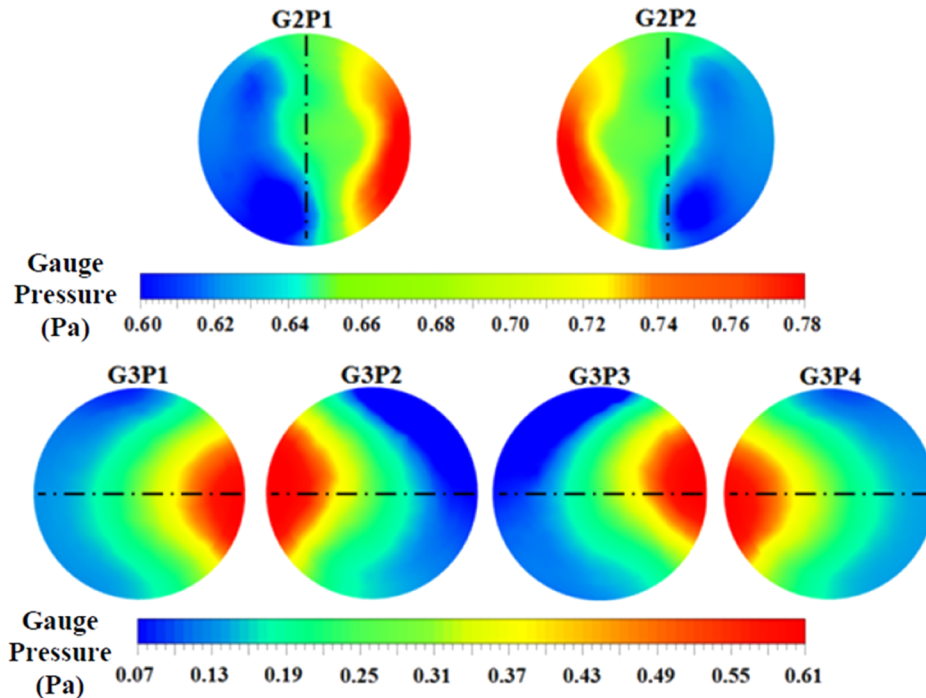


FIG. 14. Contours of gauge static pressure at the end-planes of selected branches of generations G2 and G3 in a five-generation branching network; out-of-plane configuration. — · — Traces of the downstream bifurcation ridges.

So, knowledge about the asymmetric mass-flow distribution in the branches G4B1 through G4B4 is necessary and sufficient for describing the flow in all branches of generation G4.

Figure 15 shows that the difference between the maximum and minimum flow rates in any generation in the out-of-plane configuration is much smaller than that in the in-plane configuration. As a result, the flow rates in most of the branches are almost equal to the average flow rate in the generation. Hence, the mass-flow distribution in the out-of-plane configuration (which is a more realistic representation of the bronchial tree) is found to be more uniform than that in the in-plane configuration, the greater uniformity indicating a well-functioning bronchial network.

From the above discussion, it is inferred that the generalizations made for the four-generation network (Section IV A 2) hold true for the five-generation network as well. Moreover, for a n -generation branching network in the out-of-plane configuration, the determination of the asymmetric mass-flow distribution in 2^{n-3} branches of the n th generation (i.e., $Gn - 1$) originating from the same G2 branch (and hence, lying in one of the four quarters of the three-dimensional network defined through the intersection of the longitudinal and transverse symmetry planes) is necessary and sufficient to ascertain the mass flow rate in all branches of the complete network.

C. Six-generation network (G0-G5)

The flow characteristics in six generations (G0-G5) of the branching network (both in-plane and out-of-plane configurations) according to the dimensions given in Table I are investigated here. Since the characteristics of the velocity/pressure contours on the end-planes of the branches are explained in Sections IV A and IV B, here we take a complementary approach of presenting flow solutions at the cross-sectional plane just at the beginning of a selected bifurcation module and that at the planes marking the end of the same module. Exclusion of the straight portions of the two daughter branches in this way allows a more direct assessment of the role of the bifurcation modules themselves in enhancing the asymmetry in the flow field (since the straight portions of the daughter branches tend to create a circumferentially symmetric paraboloid velocity distribution, offsetting—often only partially—the asymmetry existing at the beginning of the straight portions).

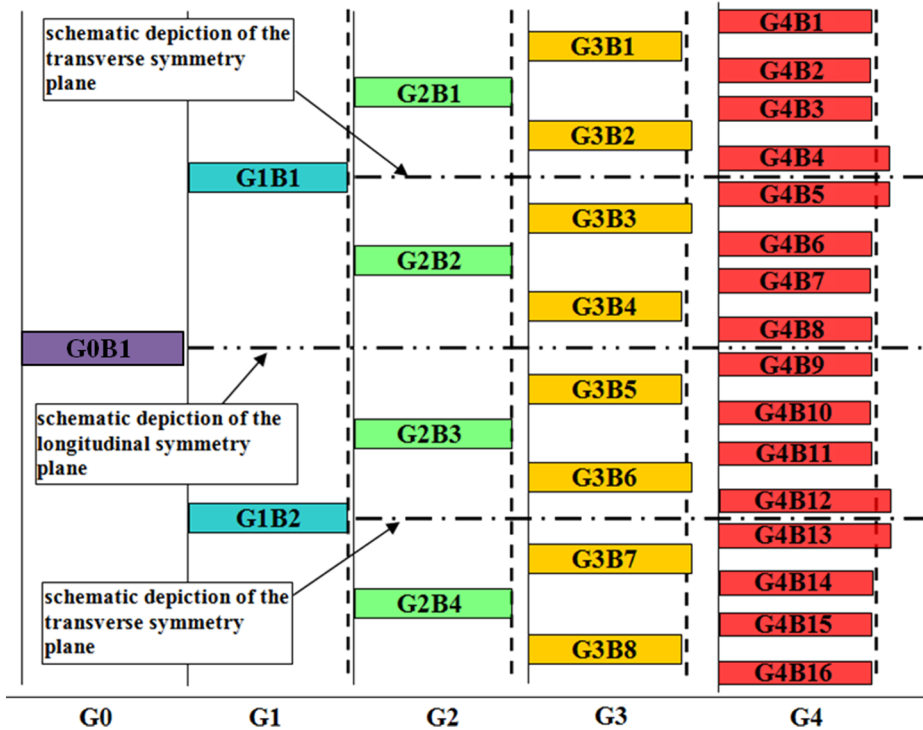


FIG. 15. Mass flow rates in all the branches in a five-generation branching network; out-of-plane configuration. [The horizontal distance between a solid vertical line (representing the start of a generation) and the following dashed line indicates the average mass flow rate per branch of the generation.]

The bifurcation modules connecting the G4 and G5 branches in the G0-G5 network are selected for the above purpose. In addition to this, the mass-flow distribution among the branches of generation G5 for both the in-plane and the out-of-plane configurations is shown here.

1. In-plane configuration (G0-G5)

Figure 16 shows the contours of velocity magnitude at the beginning (sub-plot (a)) and end (sub-plot (b)) cross-sectional planes of the bifurcation modules connecting the G4 and G5 branches in the in-plane configuration of the G0-G5 network. The representational convention for sub-plot (a) is adopted such that the trace of the downstream bifurcation ridge appears as a vertical line on the cross section. The representational convention for sub-plot (b) is adopted such that the plane containing the centrelines of the G5 branches and their corresponding mother branches intersects the cross-sectional plane along a horizontal line in the diagram. It has been established that for the in-plane configuration, the velocity contours in the branches lying on one side of the longitudinal symmetry plane are all different. Consequently, solutions in all 8 G4 branches in sub-plot (a) and those in all 16 G5 branches in sub-plot (b) are different from each other. For every branch shown here, there is one (and one only) more branch (not shown in this figure) in the same generation in which the flow solution is replicated in entirety. Moreover, the velocity contours are symmetric about a horizontal centreline on the cross section (which represents the meridional plane). The role of the bifurcation module in enhancing the asymmetry in the flow field is expressed by the fact that although the contours at the beginning of the module (sub-plot (a)) bear some similarities, those at the end of the modules (sub-plot (b)) are visibly different from one another.

Figure 17 shows the mass flow rates in the branches of generation G5 for the in-plane configuration. As discussed in the case of G0-G3 and G0-G4 networks, the flow distribution in the G0-G5 network is symmetric about the longitudinal symmetry plane (represented by the dashed line). Therefore, in order to ascertain the mass flow rates in all branches of the complete network, it is

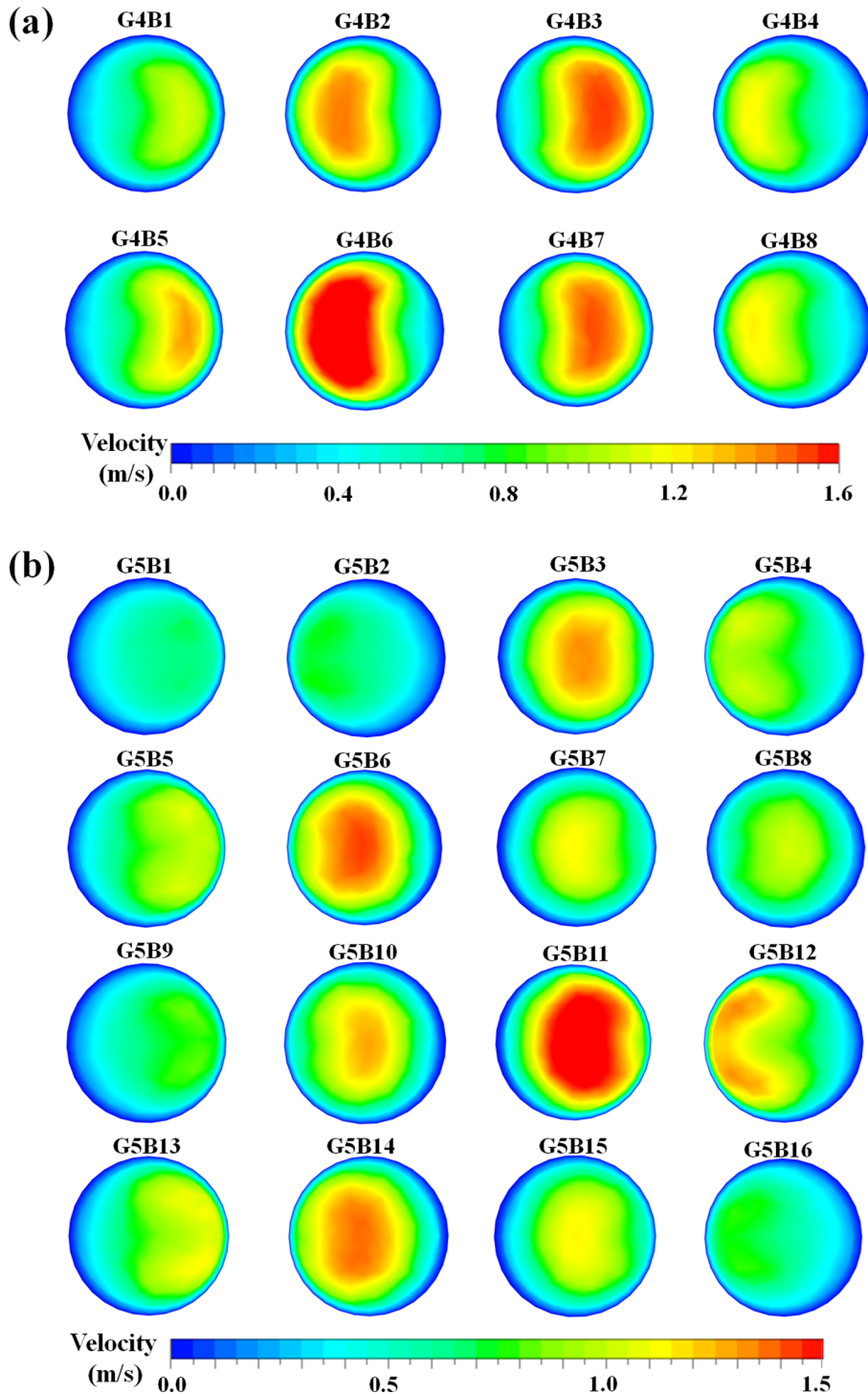


FIG. 16. The role of bifurcation modules in enhancing flow asymmetry. (a) Velocity contours at the beginning of bifurcation modules connecting branches in G4 and the corresponding daughter branches in G5 of the in-plane configuration. (b) Velocity contours at the ends of the same bifurcation modules.

necessary and sufficient to determine the mass-flow distribution in the branches on any one side of the longitudinal symmetry plane. It was seen in Figure 13 that the maximum and minimum mass flow rates in generation G4 (considering only the branches on one side of the longitudinal symmetry plane) occur in branches G4B6 and G4B1, respectively. Figure 17 shows that the maximum flow

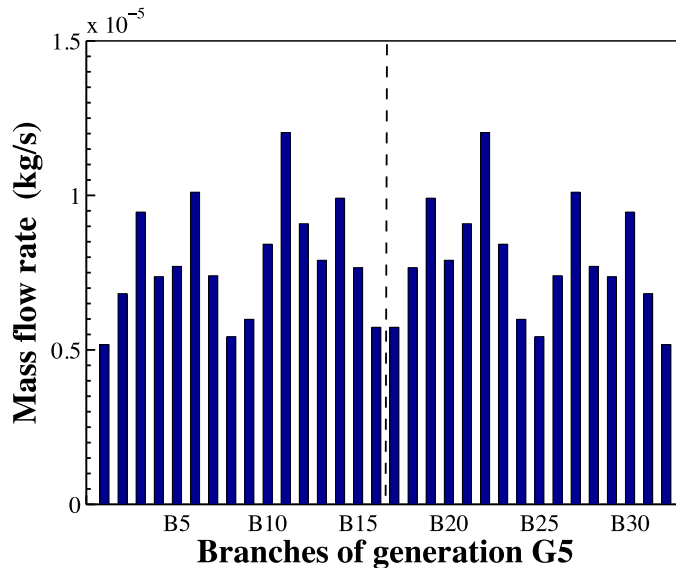


FIG. 17. The asymmetric mass-flow distribution in the branches of generation G5 in a six-generation branching network; in-plane configuration. - - - Schematic depiction of the longitudinal symmetry plane dividing the geometry into two parts showing similar flow features.

rate in generation G5 occurs in branch G5B11. This may be attributed to the fact that it receives its flow from the region of G4B6 that is aligned with the inner edge of the bifurcation module just upstream of G4B6. Figure 17 also shows that the minimum flow rate in generation G5 occurs in branch G5B1. This may be attributed to the fact that it receives its flow from the region of G4B1 that is aligned with the outer edge of the bifurcation module just upstream of G4B1.

2. Out-of-plane configuration

Figure 18 shows the contours of velocity magnitude at the beginning (sub-plot (a)) and end (sub-plot (b)) cross-sectional planes of the bifurcation modules connecting the G4 and G5 branches in the out-of-plane configuration of the G0-G5 network. The representational convention adopted for this figure is the same as that for Figure 16. It has been established that for the out-of-plane configuration, the velocity contours in the branches lying in a quarter of the network formed through the intersection of the longitudinal and transverse symmetry planes are all different. Consequently, solutions in all 4 G4 branches shown in sub-plot (a) and those in all 8 G5 branches in sub-plot (b) are different from each other. For every branch shown here, there are three (and three only) more branches (not shown in these figures) in the same generation in which the flow solution is replicated in entirety.

A comparison of Figures 16 and 18 shows that the velocity contours for the in-plane configuration are symmetric about a horizontal line in the diagram, while there is no line of symmetry for those in the out-of-plane configuration. However, the previous comment is true at the start-plane as well as at the end-planes of any selected bifurcation module. On the other hand, the role of the bifurcation module itself in creating asymmetry can be understood by noting that the qualitative difference in the flow field between any two G5 branches of the same mother branch is greater in the in-plane configuration (Figure 16(b)) than that in the out-of-plane configuration (Figure 18(b)). Quantitative measures introduced in Section IV D will also demonstrate that the bifurcation modules enhance the asymmetry in the flow field to a greater extent in the in-plane than in the out-of-plane configuration.

The mass flow rates in the branches of generation G5 for the out-of-plane configuration are shown in Figure 19. As discussed in the case of G0-G3 and G0-G4 networks, the flow field in

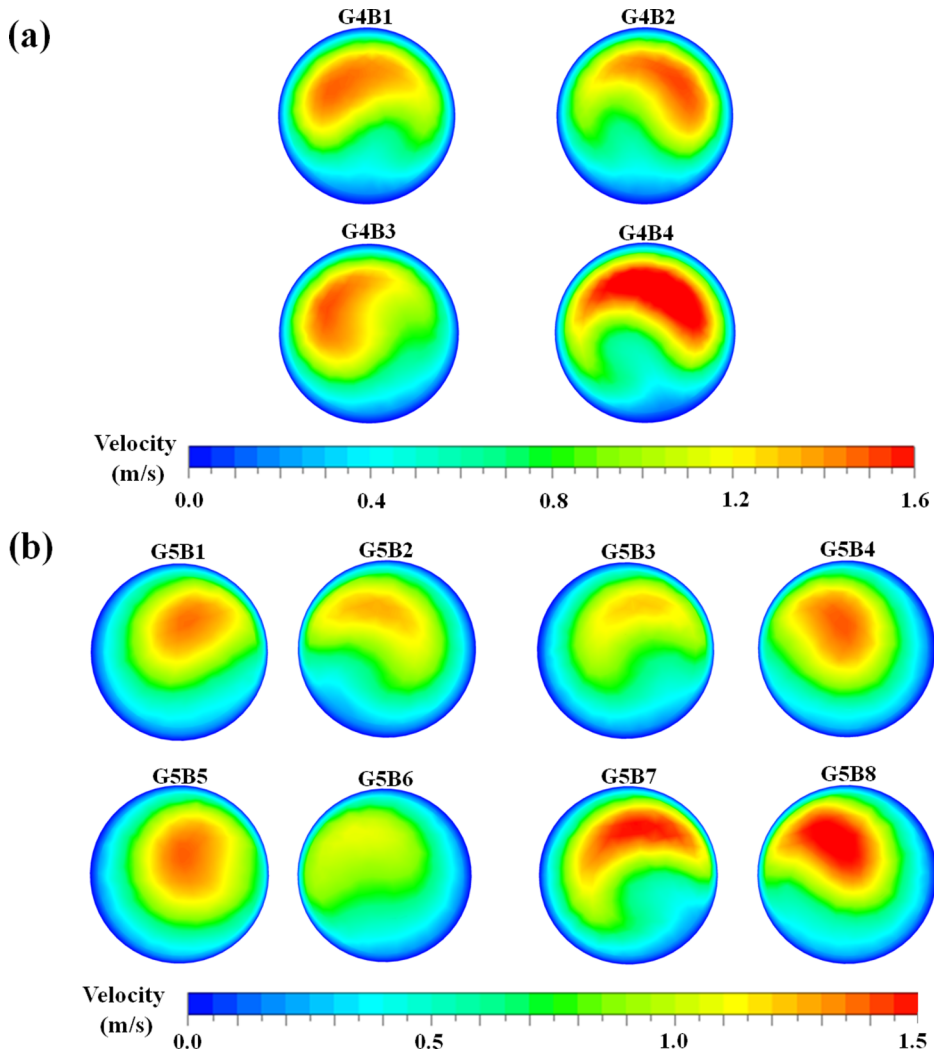


FIG. 18. The role of bifurcation modules in enhancing flow asymmetry. (a) Velocity contours at the beginning of bifurcation modules connecting branches in G4 and the corresponding daughter branches in G5 of the out-of-plane configuration. (b) Velocity contours at the ends of the same bifurcation modules.

this branching network is such that it is necessary and sufficient to determine the mass flow rates in the eight branches originating from the same G2 branch (and hence, lying in any one quarter of the network defined by the intersection of the longitudinal and transverse symmetry planes). It was seen in Figure 15 that the maximum mass flow rate among the branches of generation G4 originating from branch G2B1 occurs in branch G4B4. Figure 19 shows that the maximum flow rate in generation G5 (considering only the branches originating from G2B1) occurs in branch G5B7 which receives its flow from G4B4. A direct comparison of Figures 17 and 19 shows that the non-uniformity in the mass-flow distribution (indicated by the difference between the maximum and minimum flow rates in a generation) is much smaller in the out-of-plane configuration as compared to that in the in-plane configuration.

The above generalizations made for the G0-G5 network are thus consistent with what were established for the G0-G3 and G0-G4 networks in Secs. IV A and IV B. The non-uniformity in the mass-flow distribution is greater in the apparently simple in-plane configuration as compared to the more complex out-of-plane configuration. Sec. IV D quantifies the non-uniformity and investigates its evolution down the generations for both configurations.

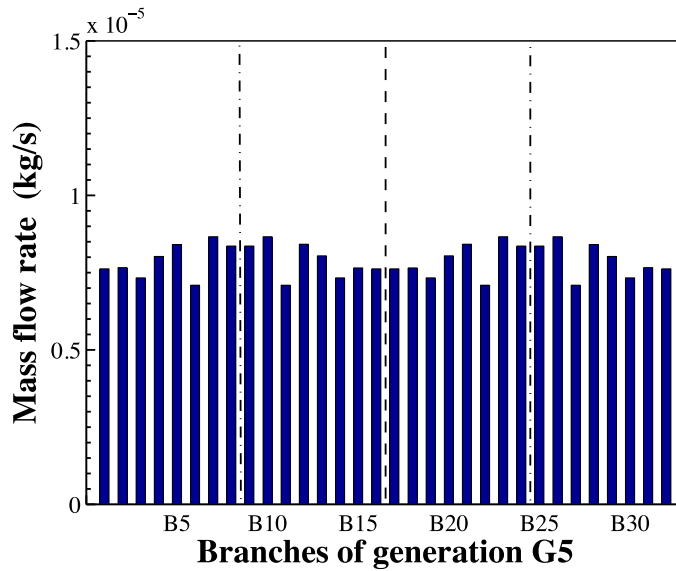


FIG. 19. The asymmetric mass-flow distribution in the branches of generation G5 in a six-generation branching network; out-of-plane configuration. - - - Schematic depiction of the longitudinal symmetry plane dividing the geometry into two parts showing similar flow features. - · - · Schematic depiction of the transverse symmetry plane which further divides the geometry resulting into four parts which possess similar flow features.

D. Evolution of flow asymmetry

It has been explained previously how the effects of flow path curvature, flow division, and inertia of the flow lead to non-uniform flow distribution in a symmetric branching network based on regular dichotomy. A new concept called “degree of mass-flow asymmetry” (δ_{Gn}) is introduced here as a simple quantitative measure of the non-uniformity (asymmetry) in the mass flow rates in various branches of a particular generation. It is defined as the ratio of the difference between the maximum and minimum flow rates in the branches of a particular generation to the average flow rate per branch in that generation. It should be kept in mind that, since there are 2^n number of branches in generation Gn , the average mass flow rate per branch halves in each successive generation. The average mass flow rate per branch in generation Gn is given by $\dot{m}_{Gn,avg} = \frac{1}{2^n} \sum_{k=1}^{k=2^n} \dot{m}_{Gn,k}$. The degree of mass-flow asymmetry in generation Gn can therefore be determined from $\delta_{Gn} \equiv (\dot{m}_{Gn,max} - \dot{m}_{Gn,min})/\dot{m}_{Gn,avg}$. The average mass flow rate $\dot{m}_{Gn,avg}$ depends only on the generation number n and not on the configuration (i.e., whether in-plane or out-of-plane). Figure 20 shows how the degree of mass-flow asymmetry varies in the successive generations of the G0-G5 network. Three general behaviours may be noted. First of all, the asymmetry in mass-flow distribution grows in each successive generation (starting from generation G2 for in-plane and G3 for out-of-plane configurations, the fluid dynamic reasons for this difference between the two configurations having been explained in Section IV A 2). Second, the degree of mass-flow asymmetry is greater for the in-plane configuration as compared to the out-of-plane configuration, with the difference between the asymmetries in the two configurations increasing down the generations. The delay in the onset of asymmetry in the out-of-plane configuration is partly responsible for the low value of δ_{Gn} as compared to the in-plane configuration. The complementary part of the explanation lies in the fact that, in the out-of-plane configuration, the fresh generation of asymmetry in two successive generations Gn and $Gn + 1$ takes place about two mutually perpendicular planes, resulting in a lower cumulative effect. Third, for the in-plane configuration, the degree of mass-flow asymmetry can be very large. As an example, Figure 20 shows that its value in the G5 branches is close to unity. This indicates that the difference between the maximum and minimum flow rates is nearly the same as the average mass flow rate per branch in generation G5. Such a high level of non-uniformity in the flow distribution, developed just in the

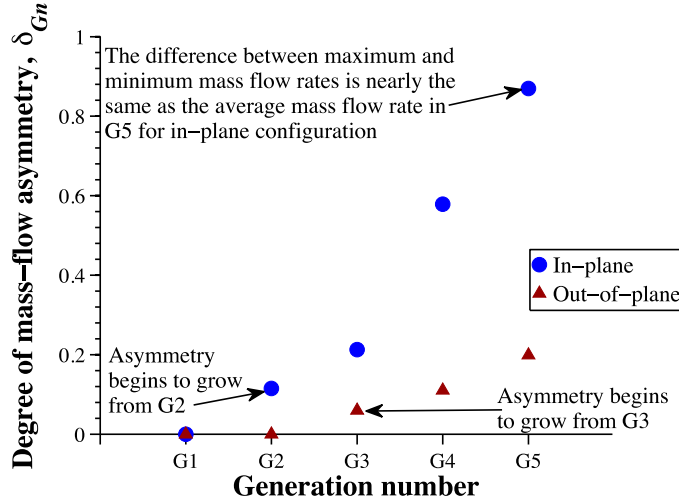


FIG. 20. Evolution of the degree of mass-flow asymmetry δ_{Gn} with increasing generation number for both in-plane and out-of-plane configurations.

first six generations of a network formed by each branch bifurcating into two geometrically similar daughter branches, seems extra-ordinary.

The “degree of mass-flow asymmetry” δ_{Gn} gives a measure of the difference between the maximum and minimum mass flow rates in a generation. In order to quantify the deviation of the flow rates in all the branches of a generation from the average flow rate per branch in that generation, a “scaled standard deviation of mass-flow distribution” (δ_{SD}) is defined as the ratio of the standard deviation of the mass flow rates in all branches of a generation to the average flow rate per branch in that generation. The value of this scaled standard deviation for generation Gn can there-

fore be determined from $\delta_{SD} \equiv \sqrt{\frac{1}{2^n} \sum_{i=1}^{i=2^n} (\dot{m}_{Gn,i} - \dot{m}_{Gn,avg})^2} / \dot{m}_{Gn,avg}$. The value of mass flow rate in an individual branch $\dot{m}_{Gn,i}$ depends on the configuration (i.e., in-plane or out-of-plane) but the average mass flow rate $\dot{m}_{Gn,avg}$ depends only on the generation number n and not on the configuration. Table IV shows the variation of δ_{SD} with generation number for both in-plane and out-of-plane configurations. As in the case of δ_{Gn} , it is found that δ_{SD} also increases in each successive generation (starting from generation G2 for in-plane and G3 for out-of-plane configurations), and the values of δ_{SD} is significantly greater in the in-plane configuration than that in the out-of-plane configuration.

Other than the mass-flow distribution in the branches of a generation, another symmetry feature of the flow field, viz., that in the flow solutions on any cross-sectional plane of a particular branch is also explored in this paper. It is established that, in general, for the in-plane configuration, the flow solution on any cross-sectional plane is symmetric with respect to the centreline which is formed

TABLE IV. Variation of the scaled standard deviation of mass-flow distribution δ_{SD} with increasing generation number.

Generation number	Scaled standard deviation of mass flow distribution δ_{SD}	
	In-plane configuration	Out-of-plane configuration
G1	0	0
G2	0.0576	0
G3	0.0781	0.0299
G4	0.1853	0.0454
G5	0.2323	0.0663

through the intersection of the cross-sectional plane and the meridional plane (see Figures 5, 6, 12, and 16). From generation G2 onward for the out-of-plane configuration, there exists no line on any cross section of a particular branch, about which the flow solution is symmetric (see Figures 9, 10, 14, and 18). So, in this respect, the flow in in-plane configuration appears more symmetric. On the other hand, the solution in any one branch is replicated in three other branches of that generation for out-of-plane configuration (from G2 onward), whereas the solution in any one branch is replicated only in another branch of that generation for in-plane configuration. In this respect, the flow in out-of-plane configuration is more symmetric. The question of the evolution of flow asymmetry in a branched network is thus complex.

E. Effect of the extent of the branching network under consideration

Figures 21(a)–21(c) are drawn, respectively, for G0-G3, G0-G4 and G0-G5 networks. The diagrams exhibit some similarities in the overall qualitative features. As an example, it may be seen that the locations where maximum and minimum pressures occur are similar in the three sub-plots. A quantitative comparison, however, is made among the flow features at a fixed location in the three branching networks (in-plane configuration), so as to understand how the flow characteristics change due to changes in the extent of the branching network under consideration. The fixed location is selected such that it is a part of all three networks (the selection is thus limited by the smallest network G0-G3). A plane located in the bifurcation module just downstream of the branch G2B2 (indicated in the schematic in Figure 21) is set as the fixed location to be used for the comparison of flow features. While the selected plane is only one generation of branches upstream of the exit of the domain (where the gauge static pressure is set to zero) for the G0-G3 network, it is two and three generations upstream of the exit for the G0-G4 and G0-G5 networks, respectively. The three branching networks are identical from the inlet to the end of generation G3 (where the G0-G3 network terminates) and therefore the effect of the location of the inlet on the flow features at the selected plane is identical for all three networks. The selection of the particular plane is based on the following two facts: (i) The plane is located sufficiently close to the exit of the domain (limited by the smallest network) such that the effect of the exit condition is felt by the fluid at the location. (ii) The maximum flow rate for the in-plane configuration of branching network is found along this flow path (Figure 13) and hence the differences (if any) in the flow features are expected to be maximum on planes along this path.

The three subplots of Figure 21, viz., parts (a), (b) and (c) show differences demonstrating the dependence of the quantitative flow solutions on the extent of the branching network under consideration. As an example, the maximum, minimum, and average values of the gauge static pressure on the selected plane are all different for the three networks. It is found that, out of the three networks considered, the average value of the gauge static pressure on the selected plane is the lowest for the G0-G3 network (where the selected plane is closest to the exit at which the boundary condition is applied), while it is the highest for the G0-G5 network (where the selected plane is farthest from the exit). The overall pressure drop from the trachea to the end of branch G2B2 (where the pressure contours are shown in Figure 21) is about 1.4 Pa. Therefore, the quantitative differences in the pressure levels between Figures 21(a)–21(c) are significant in terms of the computed overall pressure drop. It is expected that this difference in predicted values of pressure (or other flow variables) at a given location would grow as the extent of the branching network under consideration is increased further.

Previous numerical studies^{7,8} that have attempted to calculate the flow field by dividing the network into computational modules (comprising 3 or 4 generations) have used pressure boundary condition separately at the exits of each module. The modules are thought to be arranged in series and parallel like the analogous arrangement of resistances in an electrical circuit. In this way, Ref. 7 claims to have gone up to generation 23 and Ref. 8 up to generation 16. It is difficult to follow all the implementation details from these references and the accuracy of their quantitative flow solutions has not been assessed by comparing with a benchmark CFD simulation for the entire network taken together. Figure 21 of the present paper shows that the quantitative flow solutions obtained by using such pressure boundary conditions depend on the extent of the computational domain. The

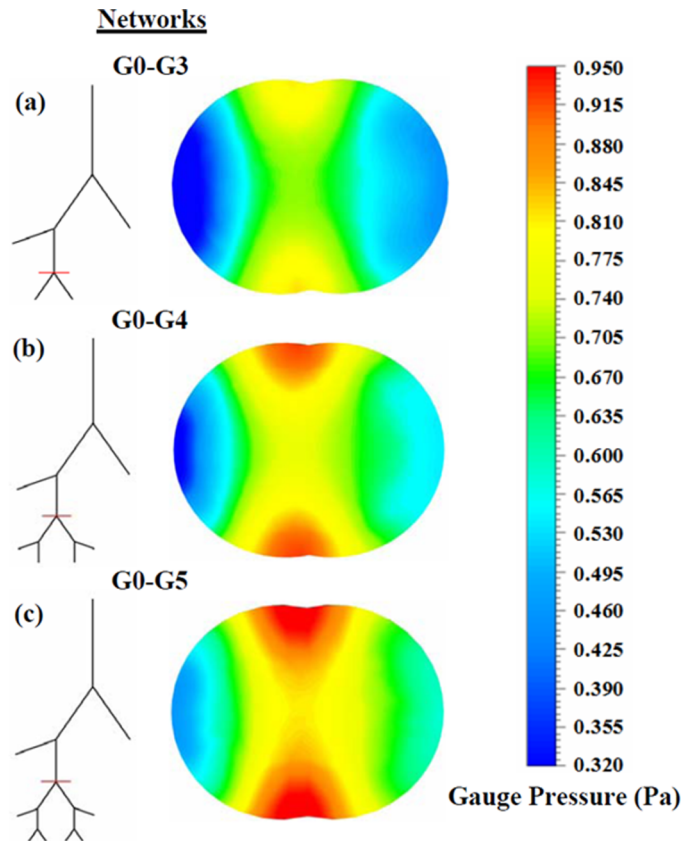


FIG. 21. Contours of gauge static pressure at the end of branch G2B2 (marked in the schematics of the network) for the three branching networks considered; in-plane configuration. (a) G0-G3, (b) G0-G4 and (c) G0-G5.

deviation of the modular flow solutions from the actual solution for the entire network can be large, particularly when the size of the module is small.

Other than the modular approach, a truncation approach is also suggested in the literature, e.g., by using a method that involves truncation of one of the two daughter branches after each bifurcation,³¹ or truncation of some of the branches in a particular generation.⁹ However, it has been established here that the geometrical symmetry of the network considered in Refs. 9 and 31 (each bifurcation dividing into two geometrically similar branches) does not automatically imply symmetry in the flow field. Asymmetry in the flow field is generated due to flow path curvature, flow division at a bifurcation, and inertia of the flow, and the flow field in the geometrically symmetric model becomes highly asymmetric, with a highly non-uniform flow distribution. Hence, finding appropriate boundary conditions at the truncated outlets will be a challenge. The detailed consideration of symmetry (or asymmetry) given in this paper is thus important in future endeavours to reduce computational resource and time for flow simulations of a branched network.

There are at least three issues with the modular or truncation approach: (i) The difficulty of combining generations in series is highlighted in Figure 21. (ii) The difficulty of combining all modules of a level in parallel is that the flow solutions in all modules of a given level are not the same, as demonstrated in this paper. Hence, the question remains how to fix the appropriate (different) outlet boundary conditions for the outlets of the modules, belonging to the same generation. (iii) Our experience shows that attempts to construct a symmetric bronchial tree with all branches included, based on Weibel's data, usually fails after a few generations because of the intersection of branches (the generation number, at which intersection occurs, depends on the bifurcation angle for both configurations and also on the rotation angle for the out-of-plane configuration, and branching

without intersection can continue up to a greater number of generations in the out-of-plane configuration). A modular/truncation approach may miss this point and one may present solutions for the arrangement of branches up to a large number of generations, even though the physical construction of the bronchial tree up to that many generations is not possible.

Guha³ discussed in detail the qualitative physics of deposition in the respiratory tract using semi-empirical methods. He also presented Eulerian and Lagrangian CFD methods for computing transport and deposition of particles. An accurate computation of deposition depends on an accurate determination of the fluid flow field. The present fluid dynamic results are steps towards establishing a thorough understanding of the three-dimensional flow in bifurcating geometries.

V. CONCLUSION

In the present study, a systematic computational method has been adopted to develop a comprehensive understanding of the fluid dynamics governing the flow in complex three-dimensional branching networks (the geometry and dimensions for the example computations being based on the human bronchial tree). Both in-plane and 90° out-of-plane configurations have been considered here in order to determine the effect of the three-dimensional arrangement of the branches on the flow characteristics. The applied numerical technique has been validated by comparisons with previously published experimental and numerical work. Separate simulations have been performed for networks comprising four, five, and six generations of branches. Computation of six generations of branches (involving 63 straight portions and 31 bifurcation modules) in one go poses computational challenges that are rarely taken in the literature.

The present computations show that solutions, such as the velocity or pressure at a given location of the network, depend on the extent (e.g., four, five, or six generations) of the network under consideration. This suggests that the modular approach often used in the literature, in which solutions in the full network are constructed by determining solutions in sequentially arranged small segments through a series of separate CFD simulations, would not produce the same flow solutions obtained by a single CFD simulation for the entire network, unless appropriate boundary conditions can be found for the intermediate boundaries.

It is shown that apparent symmetry in the geometry of any two branches does not automatically imply symmetry in the flow field in those two branches. The combined effects of flow path curvature in the bifurcation module, flow division at a bifurcation, and inertia of the flow result in skewed velocity profiles (with maximum velocity near the inner edge of a bifurcation) in the daughter branches even when the velocity field in the mother branch is symmetric about the bifurcation ridge between that mother and its daughter branches. Viscous effects try to establish a circumferentially symmetric paraboloid velocity profile in the straight portion of a branch but usually its length is insufficient for the complete removal of asymmetry, and the flow encounters the next bifurcation module where further asymmetry is introduced. Thus, even though each bifurcation appears to divide into two geometrically similar branches, the flow distribution is non-uniform. This places a serious obstacle to the truncation approach advocated in the literature, since it is difficult to find appropriate boundary conditions at the truncated branches.

With the help of velocity contours, pressure contours, and distribution of mass flow in each branch, a qualitative and quantitative study is performed on the nature and evolution of flow asymmetry. The computations show that the degree of mass-flow asymmetry (δ_{Gn}) as well as the scaled standard deviation of mass-flow distribution (δ_{SD}) is smaller for the out-of-plane configuration (which is a more realistic model of a human bronchial tree) as compared to that for the in-plane configuration. It may appear surprising at the first sight that the mass-flow asymmetry is significantly greater in a network which is apparently simpler geometrically. The mass-flow asymmetry grows in each successive generation (starting from generation G2 for in-plane and G3 for out-of-plane configurations). Other than the mass-flow distribution in the branches of a generation, another symmetry feature of the flow field, viz., that in the flow solutions on any cross-sectional plane of a particular branch is also explored in this paper. It is established that, in general, for the in-plane configuration, the flow solution on any cross-sectional plane is symmetric with respect to

the centreline which is formed through the intersection of the cross-sectional plane and the meridional plane (see Figures 5, 6, and 12). From generation G2 onward for the out-of-plane configuration, there exists no line on any cross section of a particular branch, about which the flow solution is symmetric (see Figures 9, 10, and 14). So, the question of the evolution of flow asymmetry in a branched network is complex.

It is established that, in spite of the above-mentioned complexity, there also exists a systematic order such that it is possible to ascertain the flow field in all branches of a particular generation by determining the flow field in some systematically selected branches of that generation. The flow features in the in-plane configuration are symmetric about the longitudinal symmetry plane (defined in Section III A), and hence, the determination of the flow field in the branches on any one side of that plane is necessary and sufficient to ascertain the flow characteristics in the complete network. The flow features in the out-of-plane configuration, on the other hand, are such that the determination of the flow field in the branches in any one of the four quarters formed through the intersection of the longitudinal and transverse symmetry planes (defined in Section III B) is necessary and sufficient to ascertain the flow characteristics in the complete network. Such order, in a complex flow field with growing mass-flow asymmetry in the flow direction, indicates a possible route to the saving of computational resource and time.

- ¹ J. J. Murray, A. Guha, and A. Bond, "Overview of the development of heat exchangers for use in air-breathing propulsion pre-coolers," *Acta Astronaut.* **41**(11), 723–729 (1997).
- ² A. Guha, "A unified Eulerian theory of turbulent deposition to smooth and rough surfaces," *J. Aerosol Sci.* **28**(8), 1517–1537 (1997).
- ³ A. Guha, "Transport and deposition of particles in turbulent and laminar flow," *Ann. Rev. Fluid Mech.* **40**, 311–341 (2008).
- ⁴ E. R. Weibel, "Geometric and dimensional airway models of conductive, transitory and respiratory zones of the human lung," in *Morphometry of the Human Lung* (Springer, Berlin, Heidelberg, 1963), pp. 136–142.
- ⁵ T. Heistracher and W. Hofmann, "Physiologically realistic models of bronchial airway bifurcations," *J. Aerosol Sci.* **26**(3), 497–509 (1995).
- ⁶ K. Horsfield, G. Dart, D. E. Olson, G. F. Filley, and G. Cumming, "Models of the human bronchial tree," *J. Appl. Physiol.* **31**(2), 207–217 (1971).
- ⁷ N. Nowak, P. P. Kakade, and A. V. Annapragada, "Computational fluid dynamics simulation of airflow and aerosol deposition in human lungs," *Ann. Biomed. Eng.* **31**(4), 374–390 (2003).
- ⁸ C. Kleinstreuer and Z. Zhang, "An adjustable triple-bifurcation unit model for air-particle flow simulations in human tracheobronchial airways," *J. Biomech. Eng.* **131**(2), 021007 (2009).
- ⁹ D. K. Walters and W. H. Luke, "A method for three-dimensional Navier–Stokes simulations of large-scale regions of the human lung airway," *J. Fluids Eng.* **132**(5), 051101 (2010).
- ¹⁰ Y. Zhao and B. B. Lieber, "Steady inspiratory flow in a model symmetric bifurcation," *J. Biomech. Eng.* **116**(4), 488–496 (1994).
- ¹¹ Y. Zhao and B. B. Lieber, "Steady expiratory flow in a model symmetric bifurcation," *J. Biomech. Eng.* **116**(3), 318–323 (1994).
- ¹² Y. Zhao, C. T. Brunskill, and B. B. Lieber, "Inspiratory and expiratory steady flow analysis in a model symmetrically bifurcating airway," *J. Biomech. Eng.* **119**(1), 52–58 (1997).
- ¹³ M. Tadjfar and F. T. Smith, "Direct simulations and modelling of basic three-dimensional bifurcating tube flows," *J. Fluid Mech.* **519**, 1–32 (2004).
- ¹⁴ M. Y. Kang, J. Hwang, and J. W. Lee, "Effect of geometric variations on pressure loss for a model bifurcation of the human lung airway," *J. Biomech. Eng.* **44**(6), 1196–1199 (2011).
- ¹⁵ J. K. Comer, C. Kleinstreuer, S. Hyun, and C. S. Kim, "Aerosol transport and deposition in sequentially bifurcating airways," *J. Biomech. Eng.* **122**(2), 152–158 (2000).
- ¹⁶ C. H. Zhang, Y. Liu, R. M. C. So, and N. Phan-Thien, "The influence of inlet velocity profile on three-dimensional three-generation bifurcating flows," *Comput. Mech.* **29**(4-5), 422–429 (2002).
- ¹⁷ Y. Liu, R. M. C. So, and C. H. Zhang, "Modeling the bifurcating flow in a human lung airway," *J. Biomech.* **35**(4), 465–473 (2002).
- ¹⁸ Z. Zhang, C. Kleinstreuer, and C. S. Kim, "Flow structure and particle transport in a triple bifurcation airway model," *J. Fluids Eng.* **123**(2), 320–330 (2001).
- ¹⁹ H. Y. Luo and Y. Liu, "Modeling the bifurcating flow in a CT-scanned human lung airway," *J. Biomech.* **41**(12), 2681–2688 (2008).
- ²⁰ O. Pourmehran, T. B. Gorji, and M. Gorji-Bandpy, "Magnetic drug targeting through a realistic model of human tracheobronchial airways using computational fluid and particle dynamics," *Biomech. Model. Mechanobiol.* **15**(5), 1355–1374 (2016).
- ²¹ A. J. Banko, F. Coletti, D. Schiavazzi, C. J. Elkins, and J. K. Eaton, "Three-dimensional inspiratory flow in the upper and central human airways," *Exp. Fluids* **56**(6), 1–12 (2015).
- ²² P. W. Longest and S. Vinchurkar, "Effects of mesh style and grid convergence on particle deposition in bifurcating airway models with comparisons to experimental data," *Med. Eng. Phys.* **29**(3), 350–366 (2007).
- ²³ Solidworks, Release 2010, Dassault Systèmes SolidWorks Corporation, Waltham, USA.

- ²⁴ ANSYS Academic Research, Release 15.0, ANSYS, Inc. Canonsburg, USA.
- ²⁵ A. C. Guyton and J. E. Hall, *Textbook of Medical Physiology*, 11th ed. (Elsevier, Inc., Pennsylvania, USA, 2006).
- ²⁶ ANSYS FLUENT User's Guide, Release 15.0, ANSYS, Inc., Southpointe, 275 Technology Drive, Canonsburg, Pennsylvania, USA, 2013.
- ²⁷ D. Wright, *Human Physiology and Health* (Heinemann Educational, Oxford, UK, 2000).
- ²⁸ T. J. Barth and D. C. Jespersen, "The design and application of upwind schemes on unstructured meshes," AIAA Paper No. 89-0366, 1989.
- ²⁹ P. J. Roache, "Quantification of uncertainty in computational fluid dynamics," *Ann. Rev. Fluid Mech.* **29**(1), 123-160 (1997).
- ³⁰ J. K. Comer, C. Kleinstreuer, and Z. Zhang, "Flow structures and particle deposition patterns in double-bifurcation airway models. Part 1. Air flow fields," *J. Fluid Mech.* **435**, 25-54 (2001).
- ³¹ A. F. Tena, J. Fernández, E. Álvarez, P. Casan, and D. K. Walters, "Design of numerical model of lung by means of a special boundary condition in the truncated branches," *Int. J. Numer. Methods Biomed. Eng.* (published online).